Synthesis, Characterization and Mechanical Behaviour of Epoxy Nanocomposites Reinforced with Layered Silicates

A Dissertation Submitted

For partial fulfillment of the degree of

MASTER OF ENGINEERING

in

PRODUCTION ENGINEERING

by

Gaurav Sharma

Regd. No.801382008

Under the guidance of:

Dr. Tarun Nanda
Assistant Professor, MED
Thapar University, Patiala

Dr. Rajeev Mehta
Professor, CED
Thapar University, Patiala

to the

MECHANICAL ENGINEERING DEPARTMENT

THAPAR UNIVERSITY PATIALA-147004, PUNJAB, INDIA

July, 2015

Declaration

I hereby declare that the thesis entitled **"Synthesis, Characterization and Mechanical Behaviour of Epoxy Nanocomposites Reinforced with Layered Silicates"** is an authentic record of my study carried out as requirements for the award of the degree of Master of Engineering in Production Engineering at Thapar University, Patiala under the supervision of **Dr. Tarun Nanda**, Assistant Professor, Mechanical Engineering Department and **Dr. Rajeev Mehta**, Professor, Chemical Engineering Department, Thapar University, Patiala.

Place: TU, PATIALA
Date: 14.07.2015

Gaurav Sharma

It is certified that the above statement made by the student is correct to the best of our knowledge and belief.

Dr. Tarun Nanda
Assistant Professor
Mechanical Engineering Department
Thapar University, Patiala-147004

15/07/2015

Dr. Rajeev Mehta
Professor
Chemical Engineering Department
Thapar University, Patiala-147004

Countersigned by

Dr. S.K. Mohapatra
Sr. Professor and Head
Mechanical Engineering Department
Thapar University, Patiala-147004

Dr. S.S. Bhatia
Dean
Academic Affairs
Thapar University, Patiala-147004

Acknowledgement

On the keynote, I would like to thank Dr. Tarun Nanda, Assistant Professor, MED for all the unconditional love, care, support, enthusiasm, positive energy, and inspiration given, without which I would have never developed my keen interest in polymer-clay nanocomposites. He is the best academician I have ever met in my life and I do believe he would be the last because no one could ever be like him. My thanks also go to Dr. Rajeev Mehta, Professor, CED, a man of ideas and positive hope, for all his support, patience and sharing experience. He is the backbone of my complete research work, with his limits ranging from giving appreciation for good work to even positive criticism. My both mentors are the building blocks of my thesis as well as my life and I could never repay what they have given to me. My special thanks to all my friends who supported me throughout my thesis work with their humor, laughs, suggestions, love and patience. I could never be a more complete of a person without them as they played a very vital role in completing my student life. A very special thanks to Mr. Mohit Kumar for always being there at the tea table for discussing the important events, issues and activities of the daily life. I am indebted by the trust put by my parents and my aunt on me, along with their unconditional love, care and invaluable suggestions, especially my mother who always heard me patiently even during the stressed times of my Masters degree. Finally I am thankful to God for giving me this human form and destining me for accomplishing my righteous task in this world although till today I am still searching for the ultimate goal of my life and the reason for sending me here with a hope that I will surely be guided towards it.

Abstract

Epoxy-clay nanocomposites have been widely used in application areas like encapsulation of electronic components, industrial coatings, adhesives for bonding, engineering components in aeronautics, protective coatings, high tension electrical insulators, flooring tooling etc. The present work studies the effect of nanoclay addition on the mechanical performance of epoxy based composites. The key issues included synthesis of nanocomposites with changing nano-filler content and their subsequent characterization and evaluation of mechanical properties. Synthesis of nanocomposites comprised of a definite sequence of processing steps involving homogenization and ultrasonication of the clay-epoxy mix, so as to obtain an exfoliated or intercalated morphology. Tensile, impact and microhardness testing were evaluated according to ASTM standards D638–02a, D256–02$^{\varepsilon 1}$ and E384–10$^{\varepsilon 2}$ respectively. XRD and SEM analysis were performed to study the morphology of the prepared nanocomposites and their subsequent fracture mechanisms involved during mechanical testing. XRD results showed that all nanocomposite formulations, except 0.5 wt. % clay nanocomposite, showed peak in the diffractograms, confirming the presence of intercalated clay structures. The d-spacings for pristine clay and 1.5 wt. % clay nanocomposite were 25.07 Å and 34.02 Å respectively. The maximum value of tensile modulus was obtained corresponding to 3 wt. % clay, signifying an improvement of about 63 % as compared to neat epoxy. The peak values for tensile strength, impact strength, and microhardness were obtained corresponding to 1.5 wt. % nanoclay loading as compared to neat epoxy (signifying an improvement of about 48 %, 22 % and 45 % respectively). SEM fractography of tensile fractured surface showed that the fracture surface of neat epoxy was relatively smooth and crack propagation was largely unidirectional indicating brittle type failure. However, the fracture surface of 1.5 wt. % clay nanocomposite was rough, indicating the presence of energy absorption mechanisms like crack deflection, crack pinning, and crack arresting. But, the fractured surface of 3 wt. % clay nanocomposite showed the presence of large agglomerates leading to generation of stress concentration points and decrease in tensile strength. SEM fractography of impact fractured surface of neat epoxy showed that the crack propagation lines were nearly parallel to each other, indicating fast and brittle fracture behaviour. But, the fracture surface of 1.5 wt. % clay nanocomposite showed increased roughness and tortuosity, indicating the presence of similar energy absorption mechanisms as that for tensile fractured nanocomposite.

Table of Content

List of Figures

List of Tables

List of Acronyms

Abbreviation	Acronym
AEP	Aminoethylpiperazine
ASTM	American Society for Testing and Materials
BET	Brunauer-Emmett-Teller
CLD	Cross-link density
CLTE	Coefficient of linear thermal expansion
CMC	Ceramic-matrix composites
CPN	Cloisite epoxy nanocomposite
CTBN	Carboxyl-terminated poly (butadiene-*co*-acrylonitrile)
DDM	4,4'-diamino diphenylmethane
DGEBA	Diglycidyl ether of bisphenol A
DSC	Differential Scanning Calorimetry
DOPS	Direct optical encoding positioning system
FESEM	Field Emission Scanning Electron Microscopy
FTIR	Fourier-transform infrared
HDT	Heat deflection temperature
HNT	Halloysite nano tubler
IPDA	Isophoronediamine
MMC	Metal-matrix composites
MMT	Montmorillonite
OMMT	Organo-montmorillonite
PES	Polyethersulphone
PET	Polyethylene terephthalate
PLLA	Poly (L–lactic acid)
PLS	Polymer layered silicates
PMDC	Pulse modulated direct current

PMNC	Polymer matrix nanocomposite
PNC	Polymer nanocomposite
PVAc	Poly (vinyl acetate)
SEM	Scanning electron microscopy
TEA	Tetraethylammonium chloride
TEM	Transmission electron microscopy
TGA	Thermogravimetric analysis
ToF-SIMS	Time-of-flight static secondary ion mass spectroscopy
UTM	Universal testing machine
UV	Ultraviolet
WAXD	Wide angle X-ray diffraction
WAXS	Wide angle X-ray scattering
XRD	X-ray diffraction

Symbols

T_g = Glass transition temperature

K_{IC} = plain strain/ critical intensity factor

℃ = degree Celsius

θ = Angle

λ = Wavelength

ρ = Density

Chapter 1
Introduction

1.1 Nanocomposites

During the past decade, nanocomposites have become a new class of materials that circumvent classic composite material performance by accessing new properties and exploiting unique synergism between materials. This only occurs when the length scale of morphology and the fundamental effects associated with a property coincide in the nanoscale. Indeed, the nanoscale can lead to new phenomena, providing opportunities for novel multifunctional materials applications. The rapidly growing area of nano-engineered materials will develop many perspectives for plastics and composites dictated by the final application of the polymer nanocomposites [Kotsilkova, 2007]. Nanocomposites are composites in which at least one of the phases shows dimensions in the nanometer range [Camargo *et al.,* 2009]. What differentiates nanocomposites materials from classical composites is the degree of control of fabrication, processing and performance that can be achieved nearly down to the atomic scale. Polymer nanocomposites were first developed in the late 1980s in both commercial research organizations and academic laboratories. The term 'nanocomposites' was first used in 1984 by Roy and Komarneni to emphasize the fact that the polymeric product consisted of two or more phases each in the nanometer size range [Kotsilkova, 2007]. Since then, the term 'nanocomposites' has been universally accepted as describing a very large family of materials involving structures in the nanometer size range (e.g. 1–100 nm), where the properties are of interest due to the size of the structures, and are typically different from those of the bulk matrix. The first company to commercialize polymer/layered silicate nanocomposites was Toyota, which used nanocomposites parts in the production of their novel car models [Kotsilkova, 2007]. In mechanical terms, the nanocomposites differ from the conventional composite materials due to exceptionally high surface to volume ratio of the reinforcing phase and/or its high aspect ratio. The reinforcing material can be made up of particles (e.g. minerals), sheets (e.g. exfoliated clay stacks) or fibers (e.g. carbon nanotubes). The area of interface between the matrix and the reinforcement phase(s) is typically an order of magnitude greater than for conventional composite materials. The large amount of reinforcement surface area means that a relatively small amount of nanoscale reinforcement can have an observable effect on the macro scale

properties of the composite. Nanoparticulates may result in enhanced physical properties viz. optical properties, dielectric properties, heat resistance etc. or mechanical properties such as stiffness, strength and resistance to wear and damage.

1.2 Constituents of Nanocomposites

Nanocomposites comprise of three main functional constituents described as follows:

(a) Matrix (primary phase): The matrix (or primary phase) binds the fibers together freezing in the fiber orientation, if any. Loads applied to the composite are then transferred into the fibers, the principal load-bearing component, through the matrix, enabling the composite to withstand compression, flexural and shear forces as well as tensile loads. The matrix must isolate the fibers from each other so that they can act as separate entities. The matrix should also protect the reinforcing filaments from mechanical damage (e.g. abrasion etc.) and from environmental attack. For example, for composites like MMCs or CMCs operating at elevated temperature, the matrix needs to protect the fibers from oxidative attack [Harris, 1999]. The needs or desired properties of the matrix which are important for a composite structure are as follows [Web Reference: http://nptel.ac.in/]:

- Reduced moisture absorption.
- Low shrinkage.
- Low coefficient of thermal expansion.
- Good flow characteristics so that it penetrates the fiber bundles completely and eliminates voids during the compacting/curing process.
- Reasonable strength, modulus and elongation.
- Elastic so as to transfer loads to fibers.
- Strength at elevated temperature (depending upon application).
- Excellent chemical resistance (depending upon application).
- Easily processable into the final composite shape.
- Dimensional stability (maintain its shape).

(b) Reinforcement (secondary phase): The reinforcement (secondary phase or dispersed phase) is the load bearing constituent of a composite. It may be of nano, micro, or macro level. All the loads acting over the matrix are transferred to this reinforcement through an interface. Generally reinforcement is stiffer or harder in nature than the matrix. The

degree of reinforcement or improvement of mechanical behavior depends on strong bonding at the matrix and reinforcement interface [Smith and Hashemi, 2008].

(c) Interface: A classic definition of the interface in fiber composites is a surface formed by a common boundary of reinforcing fiber and matrix that is in contact with and maintains the bond in between for transfer of loads. It has physical and mechanical properties that are unique from those of the fiber or the matrix. Interface is the geometrical surface of the classic fiber-matrix contact as well as the region of finite volume extending therefrom, wherein the chemical, physical and mechanical properties vary either continuously or in a stepwise manner between those of the bulk fiber and matrix material [Kim and Mai, 1998]. The interface is illustrated in Fig. 1.1.

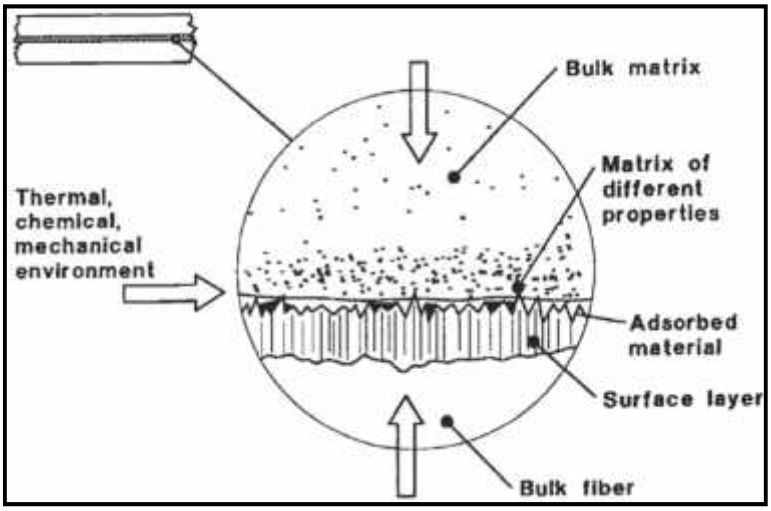

Figure 1.1: Schematic illustration of interface between fiber and matrix [Kim and Mai, 1998]

In materials where the mechanical response depends on loads being shared between two or more separate constituents or phases and where paths for the propagation of cracks will be affected by the different mechanical properties of the components, the manner in which these adhere to each other becomes an important consideration. When the strength and toughness of composites is discussed, the strength of the interfacial bond between the fibers and the matrix becomes of great importance. Interface properties depend upon the chemical and physical nature of the fibers and the matrix; there will be some modification of either chemical or physical characteristics, or both, resulting in a region which has properties quite different from those of either of the two major components. Whatever may be the origin of this region (referred to as the ‘interface’), it is the interface’s properties which determine the manner in which stresses are transferred from matrix to

fibers and, in consequence, decide many of the chemical, physical and mechanical properties of the composite [Harris,1999].

1.3 Polymer Matrix Nanocomposites (PMNCs)

Polymer nanocomposites are defined as an interacting mixture of two phases (i) a polymer matrix and (ii) a solid phase which is in the nanometer size range in at least one dimension. The solid phase is the nano filler, which can be one-dimensional (layered minerals such as clay), or two-dimensional (like carbon nanotubes, nanowires, nanofibers, cellulose whiskers etc.) or three-dimensional (spherical particles include silica nanoparticles, nanowhiskers etc.) The reinforcement of polymers using fillers, whether inorganic or organic, is common in the production of modern plastics. Conventional composites, filled with micrometer size particles, fibers or platelets, have been studied for many years for use in a large number of industrial applications. For example, composites based on thermosetting resins are widely used for structural materials, applications, such as fiber-reinforced plastics, polymer concretes, adhesives etc. Very often, the micro or the macrofiller particles are inactive and their major function is to lower the cost of the final products. In polymer composites containing inactive fillers, the most important factors governing the properties are the shape, size and distribution of filler, whereas the chemistry and surface morphology play a minor role. In contrast, polymer composites containing active fillers display a reinforcing effect of the filler on mechanical properties, depending mostly on the polymer-filler interactions and morphology of the matrix polymer. In general, polymers with active fillers of micrometer size demonstrate improved hardness but their elastic and impact properties become worse due to stress concentration resulting from the presence of filler particles. Moreover, conventional micrometer size fillers have relatively high density (~ 2–4 g/cm^3) compared to low density of the matrix polymer (~ 0.8–1.2 g/cm^3). In order to gain a reinforcing effect of engineering polymers, a large amount (30–60%) of fillers is traditionally used in composites, leading to about 20–30% increase in the weight of the final material. Besides, processability worsens as filler content increases. In contrast, nanocomposites show enhanced thermo-mechanical properties even with a small amount of layered silicate (≤ 5%). Polymer nanocomposites are known for their outstanding mechanical properties like high elastic modulus, increased strength, barrier resistance, flame retardancy etc. with very small addition (≤ 5 wt. %) of nano particles. This is due to the very large surface area of interaction between polymer matrix and nano filler [Kotsilkova, 2007].

1.4 Epoxy Clay Polymer-Matrix Nanocomposites

Among the different nano fillers, special attention has been paid to clays in the field of nanocomposites. Clays (layered silicates) are found to be one of the ideal nano reinforcements for polymers, because of their high intercalation chemistry, high aspect ratio, ease of availability and low cost. Among polymer layered silicate (clay) nanocomposites, epoxy based system is reported in detail, due to the ease of processing as well as its versatile applications (see section 1.4.6) in various fields [Azeez *et al.*, 2013].

1.4.1 Epoxy Resin

The term 'epoxy resin' refers to both the prepolymer and its cured resin/hardener system. Its characteristic group is a three membered ring known as epoxy, epoxide, oxirane, and glycidyl or ethoxyline group. The general representation of epoxy group is shown in Fig. 1.2.

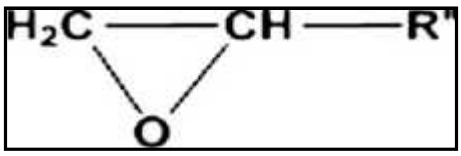

Figure 1.2: Epoxy or oxirane group [Azeez *et al.*, 2013]

This chemical structure is much strained and hence highly reactive. Epoxy resins can be cross-linked through a polymerization reaction with a hardener at room temperatures (aliphatic amines) or at elevated temperatures (aromatic amines and acid anhydrides). In general, high temperature cured resin systems have improved properties, such as higher glass transition temperature, strength and stiffness, compared to those cured at room temperatures. Epoxy resins have excellent chemical and heat resistance, high adhesive strength, good impact resistance, high strength and hardness, and high electrical insulation [Azeez *et al.*, 2013]; along with absence of byproducts/volatiles during cuing reactions; low shrinkage during cure; curing over wide temperature range; excellent resistance to chemical and solvents; excellent adhesion to a wide variety of fillers, fibers and other substrates [Mallick, 2008]. Cured epoxy resin, due to high cross-linking density, display good temperature performance. But these cured resins lack the required toughness and are very brittle [Babayan and Nguyen, 1997].

1.4.2 Clays

The commonly used layered silicates for the preparation of PLS nanocomposites belong to the same general family of 2:1 layered or phyllosilicates. Their crystal structure consists of layers made up of two tetrahedrally coordinated silicon atoms fused to an edge-shared octahedral sheet of either aluminium or magnesium hydroxide. The layer thickness is around 1nm, and the lateral dimensions of these layers may vary from 30 nm to several microns or larger, depending on the particular layered silicate. Stacking of the layers leads to a regular van der Waals gap between the layers called the *interlayer* or *gallery*. Isomorphic substitution within the layers (for example, Al^{3+} replaced by Mg^{2+} or Fe^{2+}, or Mg^{2+} replaced by Li^{1+}) generates negative charges that are counterbalanced by alkali or alkaline earth cations situated inside the galleries [Ray and Okamoto, 2003]. Such layers extend continuously in the plane constituted by the x and y axis and are stacked up in the z-axis, forming the whole crystal structure. Among the different types of clay minerals, montmorillonite is the most commonly used for preparation of polymer clay nanocomposites due to its ability to show extensive interlayer expansion or swelling because of its peculiar structure. The silicate layers of MMT are planar and having high aspect ratio and large active surface area of 700–800 m^2/g [Azeez *et al.*, 2013]. The structure of MMT is shown below in Fig. 1.3.

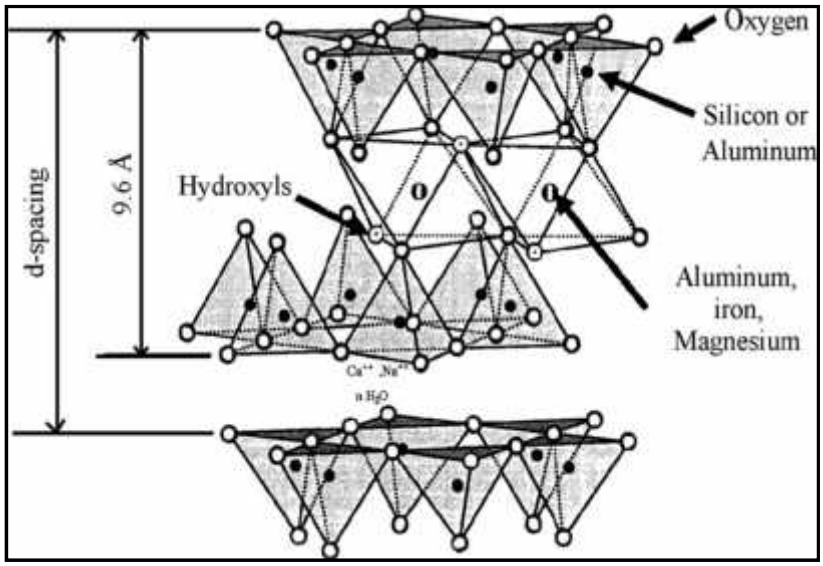

Figure 1.3: Structure of montmorillonite clay [Azeez *et al.*, 2013]

The physical mixture of a polymer and layered silicate may not form a nanocomposite. This situation is analogous to polymer blends, and in most cases separation into discrete phases takes place. In immiscible systems, which typically correspond to the more conventionally filled polymers, the poor physical interaction between the organic and inorganic components

leads to poor mechanical and thermal properties [Ray and Okamoto, 2003]. It means that clays are hydrophilic in nature. In order to make them compatible with organic polymers, the surface of the clay minerals is modified to become organophilic prior to their use. Organic cations such as an ammonium ion or phosphonium ion are the commonly used organic modifiers for clay minerals. The organic modification causes the expansion of the interlayer space and thereby increases the d-spacing to certain extent (normally over 2 nm). Thus, the organic modification favors the diffusion of polymer or its precursor into the interlayer space which means that the d-spacing increases with the organic modification of clay and it further increases when it is swelled in epoxy resin. The intercalation and exfoliation of the clay layers in the polymer matrix can be identified through WAXD and TEM [Azeez *et al.*, 2013]. The organic modification of clay is shown in the Fig. 1.4.

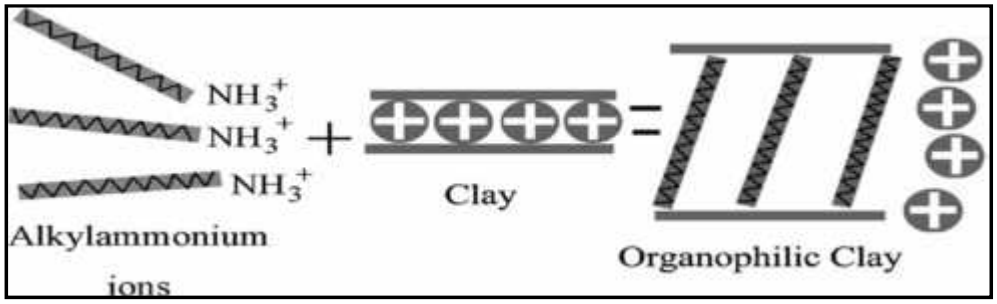

Figure 1.4: Organic modification of clay [Azeez *et al.*, 2013]

1.4.3 Structure of Polymer Clay Nanocomposites

The polymer clay nanocomposites can be divided into three categories on the basis of structure obtained (see Fig. 1.5).

(a) Phase-separated microcomposite: When the polymer is unable to intercalate between the silicate sheets, a phase-separated composite is obtained whose properties stays in the same range as traditional microcomposites [Alexandre and Dubois, 2000; Camargo *et al.*, 2009]. An improvement in modulus is normally achieved in conventional clay composites but this reinforcement benefit is usually accompanied with a deficiency in other properties such as strength or toughness [Azeez *et al.*, 2013]. On an XRD diffractogram, phase-separated nanocomposite morphology is characterized by the presence of peak, such that the 2θ position of this peak is always greater as compared to 2θ position of the nanoclay.

(b) Intercalated nanocomposites: In these nanocomposites, the insertion of the polymer matrix into the layered silicate structure occurs in a crystallographically regular fashion,

regardless of the clay to polymer ratio. Properties of these nanocomposites typically resemble those of ceramic materials [Ray and Okamoto, 2003]. A well ordered multilayer morphology built up with alternating polymeric and inorganic layers is generated. Normally, only a few molecular layers of polymer can be intercalated in these materials [Camargo *et al.,* 2009]. The d-spacing maintained is 20–30 Å [Azeez *et al.,* 2013]. On an XRD diffractogram, intercalated nanocomposite morphology is characterized by the presence of peak, such that the 2θ position of this peak is always less as compared to 2θ position of the nanoclay.

(c) Exfoliated nanocomposites: When the silicate layers are completely and uniformly dispersed in a continuous polymer matrix, an exfoliated or delaminated structure is obtained [Alexandre and Dubois, 2000]. The individual clay layers are separated in a continuous polymer matrix by an average distance that depends on clay loading. Usually, the clay content of an exfoliated nanocomposite is much lower than that of an intercalated nanocomposite [Ray and Okamoto, 2003]. The d-spacing maintained is more than 50 Å [Azeez *et al.,* 2013]. The presence of exfoliated nanocomposite morphology is characterized by the absence of any peak on XRD diffractogram.

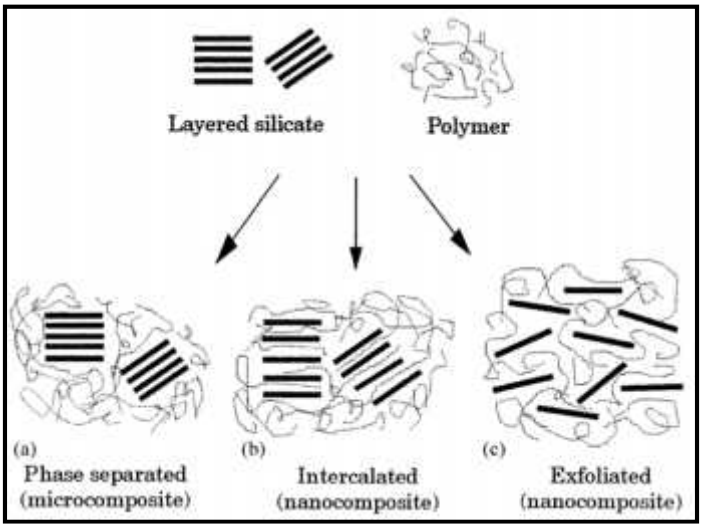

Figure 1.5: Structures in polymer clay nanocomposites [Alexandre and Dubois, 2000]

1.4.4 Mechanism of Clay Exfoliation in Polymer Clay Nanocomposites

The polymer chains, in this case the cross-linked epoxy molecules, store more energy to recoil with growing molecular weight, i.e. with the extent of curing. This energy can be expressed in terms of the value of storage modulus of cross-linking epoxy molecules. The adjacent layers of clay particles holding the polymerizing epoxy molecules within them, however, prevent recoiling of the cross-linked epoxy chains due to (1) electrostatic attractive

forces between the quaternary ammonium ions and the negatively charged clay particles and (2) the van der Waals forces between the organic fragments of the quaternary ammonium ions. Consequently, the cross-linked cannot relax, and its conformational entropy gradually increases to a critical point whereby the attractive forces balance the entropic elastic forces. Beyond this critical point, the elastic forces outweigh the attractive forces and adjacent clay layers move away from each other. However, the viscous force offered by the extragallery epoxy must be overcome for eventual separation of the clay layers. The cross-linking epoxy molecules undergo recoiling process in all cases of curing speed but have longer times available to change conformation and relax when the rate of curing is slow. Under faster curing condition, however, cured epoxy chains have very little time to experience stress relaxation and, therefore, store much more elastic energy than the chains produced under slow curing conditions. This is true for both intra- and extragallery epoxy molecules. The relaxation process of curing epoxy chains and the possibility of whether clay layers can be pushed out of the tactoids to yield exfoliated structures depend strongly on how the viscosity of extragallery epoxy offers viscous resistance to separation of clay layers. Therefore, clay layers exfoliation is difficult if the viscosity of the epoxy rises faster. The sum of viscous force and attractive forces arising due to electrostatic attraction and van der Waals force work against exfoliation, while elastic forces due to conformational entropy work for clay layer separation. If the elastic force overcomes the attractive forces and viscous forces, exfoliation of clay occurs; otherwise, intercalated clay structures, with cross-linked epoxy molecules in them, are retained in the cured system. It is worthwhile to mention that exfoliation in an uncured system is not expected as the magnitude of the entropic force responsible for separating the clay layers is small due to small size of the epoxy monomers intercalating the clay galleries [Park and Jana, 2003]. The mechanism of clay exfoliation is shown in Fig. 1.6.

The complete exfoliation of clay layers from the intercalated tactoids can be produced if the ratio of shear modulus to complex viscosity is maintained at or above 2–4 s^{-1} such as the elastic forces inside the galleries outweigh the viscous forces offered by the extragallery epoxy. So the elastic forces exerted by the cross-linking epoxy molecules inside the clay galleries push out the outermost clay layers from the tactoids against the opposing forces arising from electrostatic and van der Waals attraction and shear, the latter due to motion of clay sheets during exfoliation [Azeez *et al.*, 2013].

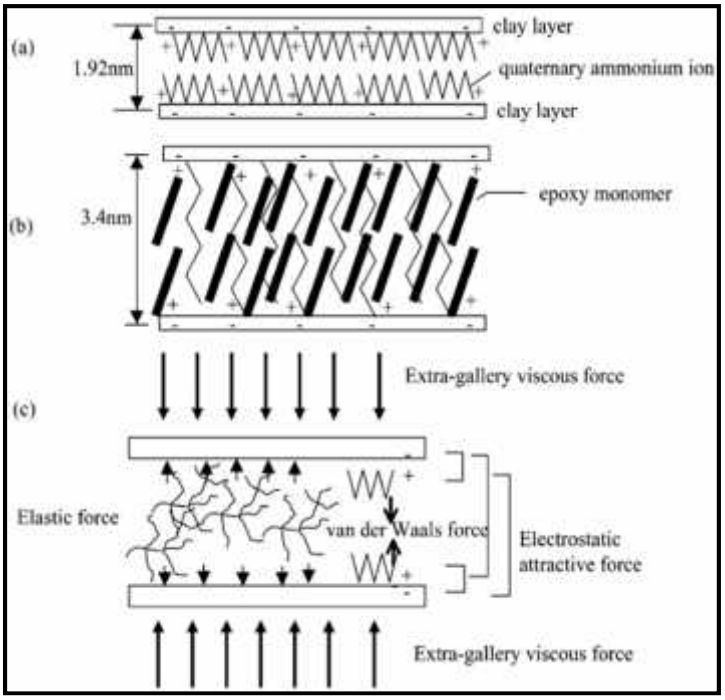

Figure 1.6: Schematic of the intercalated state and exfoliation process showing the forces acting on a pair of clay layers [Park and Jana, 2003]

1.4.5 Properties of Epoxy Clay Nanocomposites

PLS nanocomposites have proved to trigger a tremendous properties improvement of the polymers in which they are dispersed. Amongst those properties, unexpected large increase in moduli (tensile or Young's modulus and flexural modulus) of nanocomposites at filler contents sometimes as low as 1 wt. % has drawn a lot of attention. Thermal stability and fire retardancy through char formation and other interesting and widely searched properties are displayed by nanocomposites. Those new materials have also been studied and applied for their superior barrier properties against gas and vapor transmission. Finally, depending upon the type of polymeric materials, they can also display interesting properties in the frame of ionic conductivity and thermal expansion control [Alexandre and Dubois, 2000]. Epoxy-clay nanocomposites show enhanced thermo-mechanical properties even with a small amount of layered silicate i.e. ≤ 5% [Azeez *et al.*, 2013]. These enhancements are partly attributable to the extremely large particle surface area available for interaction with the polymeric matrix, coupled with a high aspect ratio between 30 and 2000 [Auad *et al.*, 2007]. Some of these improvements include higher moduli, increased strength and heat resistance, decreased flammability and gas permeability and increased biodegradability [Camargo *et al.*, 2009]. Now since our area of interest is the epoxy-clay nanocomposites hence, the various properties associated with it are presented as follows:

(a) Mechanical properties: The good dispersion of clay particles in the polymer matrix yields enhanced tensile modulus, storage modulus and tensile strength. Even though, the tensile modulus and strength tend to increase with increasing clay content [Gupta *et al.,* 2007; Hwang *et al.,* 2008; Mouloud *et al.,* 2012; Kusmono *et al.,* 2013], the increasing trend is more noticeable for the tensile modulus. The reinforcing effect of clay layers on the tensile modulus is mainly due to the high modulus and high aspect ratio of the dispersed clay layers. This provides larger interfacial interaction between the clay layers and polymer matrix. Mechanical properties of polymer-clay nanocomposites depend on the microstructure i.e. how the clay layers are dispersed in the polymer matrix [Azeez *et al.,* 2013]. But, a reduction in tensile strength, impact strength, fracture toughness as well as strain at break of the polymer clay nanocomposites with the addition of clay particles was also observed at high clay loadings [Isik *et al.,* 2003; Gupta *et al.,* 2007; Hwang *et al.,* 2008; Mouloud *et al.,* 2012; Kusmono *et al.,* 2013]. The reason is that stress concentration effect of agglomerated clay particles at higher clay contents. The agglomeration of clay particles at higher clay concentration also results in decrease in mechanical properties due to lowering of filler surface area and lower polymer/clay surface interaction. Another reason is that as the clay content increases, the viscosity of the system increases resulting in heterogeneity and nanovoids formation due to the entrapment of air bubbles during sample preparation [Azeez *et al.,* 2013].

(b) Thermal properties: Polymer clay nanocomposites are known for their high thermal stability and flame retardancy. The improved thermal stability is attributed to the action of clay layers as superior insulators and mass transport barriers to the volatile products generated during decomposition as well as assisting in the formation of char after thermal decomposition. The improved thermal stability of the clay modified epoxy systems are attributed to barrier action of hard MMT-clay nanolayers, which protect from volatilizing epoxy polymers chains present in between them and also restrict the segmental motion of the polymer networks [Azeez *et al.,* 2013]. As the polymer is exposed to heat, it will begin to decompose but, instead of forming smaller fragments and flowing/melting under heat exposure, it will instead solidify further. The now highly cross-linked material can then turn to char which slows down the rate of fuel release/pyrolysis products into the gas phase for combustion. This phenomenon creates a low heat release material since more and more of the potential carbon fuel is bound up in a form that cannot be pyrolyzed further.

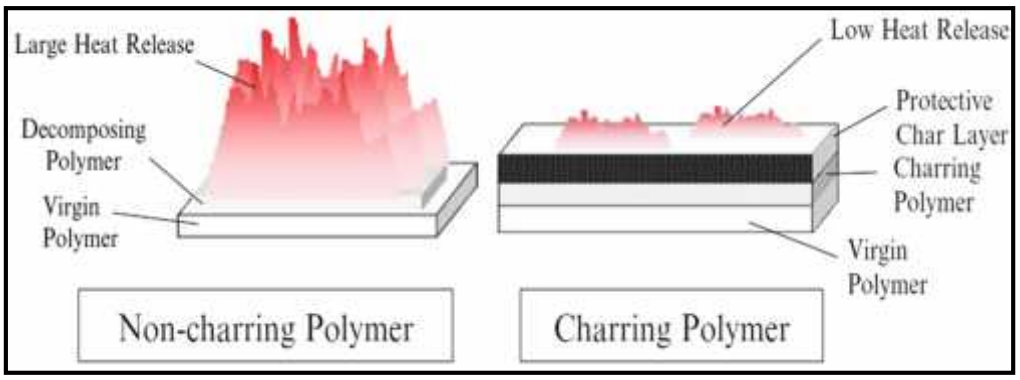

Figure 1.7: Differences in heat release caused by non-charring and charring polymers [Morgan, 2012]

In effect, char formation keeps the polymer in the condensed phase rather than allowing it to enter into the vapor phase. The formation of this char can greatly lower heat release [Morgan, 2012] as shown in the Fig. 1.7.

(c) Barrier properties: Clay layers in the polymer matrix can act as an effective barrier to the penetrants. The enhanced barrier properties of polymer nanocomposites are due to the labyrinth or tortuous path that retards the diffusion of gas molecules through the polymer matrix [Azeez *et al.*, 2013]. The labyrinth or tortuous path is shown in Fig. 1.8.

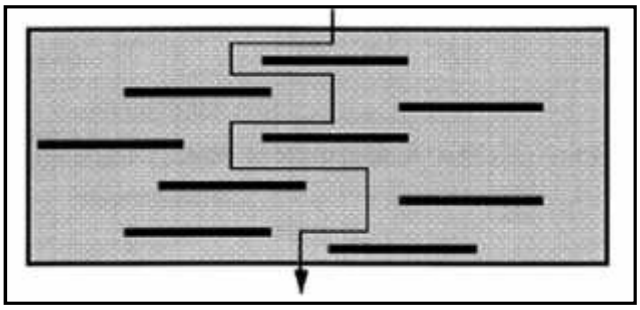

Figure 1.8: Zigzag diffusion (tortuous) pathway of a gas through clay-based polymer nanocomposites [Azeez *et al.*, 2013]

1.4.6 Applications of Polymer Clay Nanocomposites

Polymer based nanocomposites are in the forefront of applications due to their more advanced development status compared to metal and ceramic counterparts, in addition to their unique properties. The most common use of polymer-clay nanocomposites has been in mechanical reinforcement of thermoplastics, especially polyamide-6 and polypropylene. The aforementioned polyamide-6 clay nanocomposite produced by Ube/Toyota was used to replace a metal component near the engine block that yielded some weight savings. The clay in this application improved the heat distortion temperature of the material, allowing it to be used in this higher temperature applications. GM/Blackhawk has also announced

polypropylene-clay nanocomposites for automotive applications, and the clay brought an increase in flexural/tensile modulus while maintaining impact performance [Morgan, 2012]. Heat resistant polymer nanocomposites are used to make fire fighter protective clothing and lightweight components suitable to work in situations of high temperature and stress. This includes hoods of automobiles and skins of jet aircrafts, as opposed to heavier and costlier metal alloys. They can also replace corrosion-prone metals in the building of bridges and other large structures with potentially lighter and stronger capabilities. Regarding the variety of applications of polymer nanocomposites, prominent impacts over the automotive industry can be highlighted, including their use in tires, fuel systems, gas separation membranes in fuel cells and seal textiles, mirror housings on various vehicle types, door handles, engine covers, intake manifolds and timing belt covers, with some of these already being exploited. Other promising technological applications in the horizon is in air bag sensors, where nano-optical platelets are kept inside the polymer outer layer for transmitting signals at the speed of light gaining milliseconds to bring down the level of possible impact injuries. Improvements in the mechanical properties of polymer nanocomposites have also resulted in their many general/industrial applications. These include impellers and blades for vacuum cleaners, power tool housings, and mower hoods and covers for portable electronic equipment, such as mobile phones and pagers. The incorporation of nanoclay particles into thermoplastic resins has shown excellent barrier characteristics which have resulted considerable interests in food packaging applications. Specific examples include packaging of processed meats, cheese, confectionery, cereals, and boil-in-the-bag foods, also extrusion-coating applications in association with paperboard for fruit juice and dairy products, together with co-extrusion processes for the manufacture of beer and carbonated drink bottles. The use of nanocomposite formulations would be expected to enhance considerably the shelf life of many foods [Camargo *et al.*, 2009]. The aerospace applications include use of polymer-clay nanocomposites in air-frames, wing spars, spoilers, tail-plane structures, fuel tanks, drop tanks, bulkheads, flooring, helicopter rotor blades, propellers, and structural components, pressured gas containers, radomes, nose and landing gear doors, fairings, engine nacelles (particularly where containment capability is required for jet engines), air distribution ducts, seat components, access panels and so forth. Space applications offer many opportunities for employing light-weight, high-rigidity structures for structural purposes. Many of the requirements are the same as those for aeronautical structures, since there is a need to have low weight and high stiffness in order to minimize loads and avoid the occurrence of buckling frequencies. Dimensional stability is at a premium, for stable antennae and optical

platforms, for example, and materials need to be transparent to radio-frequency waves and stable towards both UV radiation and moisture [Harris, 1999]. Similarily, polymer nanocomposites also play their role in biomedical applications. For example, the screws and rods that are used for internal bone fixation bring the bone surfaces in close proximity to promote healing. This stabilization must persist for weeks to months without loosening or breaking. The modulus of the implant must be close to that of the bone for efficient load transfer. The screws and rods must be non-corrosive, nontoxic, and easy to remove if necessary. Thus, a polymer nanocomposite implant must meet certain design and functional criteria, including biocompatibility, biodegradability, mechanical properties, and, in some cases, aesthetic demands. In this direction, PLLA has widespread applications in sutures, drug delivery devices, prosthetics, scaffolds, vascular grafts, bone screws, pins, and plates for temporary internal fixation [Hule and Pochan, 2007]. Corrosion protection of metals and alloys is normally achieved by a surface coating which must resist both mechanical damage (scratching, impact, abrasion) and chemical attacks (salts, acids and bases, solvents). PNCs have improved scratch and abrasion resistance, due to their higher hardness combined with improved elastic modulus. Corrosion protection in aerospace (at normal or low temperatures, not suitable above 150 ℃) and corrosion protection of electronic circuits demand such materials [Kurahatti *et al.,* 2010]. Filament wound carbon fiber reinforced cryotanks made with epoxy nanocomposite have a fivefold lower helium leak rate than the corresponding tanks made without clay. Epoxy-clay nanocomposites have been extensively used for the structural adhesive applications, due to its potential improvement in adhesive properties with practicality and low cost. These composites are also used in high performance structural and functional applications such as laminates and composites, adhesives, sealants, tooling, molding, casting, electronics and construction [Azeez *et al.*, 2013].

1.5 Summary of the Chapter

This chapter begins with the discussion about nanocomposites and their constituents, followed by introduction to polymer matrix nanocomposites and specifically epoxy-clay polymer matrix nanocomposites. Epoxy resin and MMT are discussed in detail alongwith the structure of clay and various morphologies of epoxy-clay nanocomposites obtained after mixing (phase separated, intercalated and exfoliated). Finally, the mechanical, thermal and barrier properties of epoxy-clay nanocomposites have been discussed followed by applications of polymer-matrix nanocomposites.

Chapter 2

Literature Review

2.1 Introduction

This section presents the literature review related to epoxy resin based matrix systems with layered silicates as reinforcements. The literature review has been used to discuss the effects of different constituents, method of preparation, use of additives etc. on the mechanical and physical properties of epoxy-clay nanocomposites.

2.2 Review of Epoxy-Clay Based Nanocomposites

Park and Jana (2003) investigated the mechanism of nanoclay exfoliation in epoxy/clay nanocomposites and tested the hypothesis that the elastic forces (polymer recoiling) developed in the clay galleries during epoxy curing is responsible for exfoliation of the clay structures. Clay 1 (Cloisite 30B), Clay 2 (Cloisite Na^{+}) and Clay 3 (Clay 2 treated with n-hexadecylamine hydrochloride) were taken. Clay 1 and Clay 3 were separately intercalated by epoxy by stirring the ingredients at 80 °C for 6 h with a magnetic stirrer, and the resulting mixture was dried in a vacuum oven at 80 °C for 30 minutes. A suitable amount of curing agent was added to the epoxy-clay mixture and the ingredients were mixed further for approximately 5 minutes at 60 °C. The resultant mixture was degassed in a vacuum oven for approximately 5 minutes at 60 °C and cured in an aluminum mold. The curable epoxy mixtures without the clay were prepared by mixing the ingredients for 5 minutes at 60 °C. The curing temperature and time were varied as per curing agents. WAXD results showed that the quaternary ammonium ions increased the d-spacing in treated clay from 1.12 (for Clay 2) to 1.77 nm in Clay 1 and to 1.92 nm in Clay 3. Finally it was concluded that complete exfoliation of clay structures can be produced till elastic forces inside the galleries were prevailed by the viscous forces offered by the extra-gallery epoxy.

Yasmin *et al.* (2003) used a three-roll mill machine to exfoliate the stacked layers of silicate clay in the epoxy matrix and studied the correlation between the degree of exfoliation and the mechanical properties of the fabricated nanocomposites. The resin, hardener, accelerator (mixed in the 100:90:1 ratio) and nanoclay used were DGEBA epoxy, methyl tetrahydrophthalic anhydride, 1-Methylimidazole and, Nanomer I.28E respectively. The epoxy resin was placed between the feed and center rolls. Once the rolls started moving, the

clay particles were spread gradually on the resin to get direct and maximum contact with the rolls. This compounding was carried out at room temperature for 3 h, with a rotation speed of 500 rpm and a feed rate of 120 g/h. Then, hardener was mixed into the obtained final product at 60 ℃ for 1 h on a hot plate. After adding accelerator and mixing for few minutes, the solution was left overnight for degassing. Finally, the mixture was poured in aluminium molds and cured at 148 ℃ for 1 h. Nanocomposites were prepared with clay concentrations from 1 to 10 wt. %. WAXD patterns showed an absence of peak for 2 wt. % clay loading, which is an indicative of exfoliated structure. The nanocomposite with 1 wt. % clay showed a shallow peak with d-spacing of 3.66 nm whereas at higher clay content (> 2 wt. %) pronounced peaks were observed with d-spacing slightly lower than the composite containing 1 wt. % clay. It was observed that the modulus of the composite increases continuously with increasing concentration of clay. An improvement of about 34 % was observed just for an addition of 2 wt. % clay. However, the improvement of only 42 and 52 % for an addition of 5 and 10 wt. % clay respectively signified the decreased rate of improvement at higher concentrations. Unlike elastic modulus, nanocomposites with any clay concentration showed a lower tensile strength than the pure epoxy. SEM fractographs of 10 wt. % clay nanocomposite showed bright spots corresponding to clay aggregates and these aggregates were finely dispersed in the material which confirmed the inevitable aggregation of clay layers in the nanocomposite.

Isik *et al.* (2003) studied the effect of polyether polyol (impact modifier) and montmorillonite contents on the morphological, thermal and mechanical properties of synthesized nanocomposites. MMT and clay are mechanically stirred for 2 h at 35℃, followed by ultrasonic mixing for 30 minutes. at 47 kHz; addition of polyether polyol and mechanical stirring for 1hr; degassing; cooling at room temperature; addition of triethylenetetramine curing agent at 100:20 (DGEBA/hardener) by weight; curing at 75 ℃ for 16 h and finally post curing at 130 ℃ for 3 more hours. Specimen ASTM 638−M91a for tensile tests and ASTM D 256 for charpy impact tests were used. XRD analysis showed 2θ = 1.83, 3.82 and 4.01 nm while the Basal spacing corresponding to them are 1.83, 3.82 and 4.01 nm. SEM analysis showed that with changing montmorillonite contents (0, 1, 3, 5 wt %) and polyether polyol content (1 and 7 wt. %), the average diameter of the polyether polyol domains showed an increasing trend. DSC analysis showed that the glass transition temperature increases with the addition of montmorillonite. Young's modulus increases with increase in amount of montmorillonite at constant polyether polyol contents. XRD patterns showed that the addition

of polyether polyol impact modifier did not significantly change the basal spacing i.e. it was found 3.82 nm for nanocomposite with 3 wt. % Cloisite 30B and 4.01 nm for nanocomposite with 3 wt. % Cloisite 30B and 7 wt. % polyether polyol. Thus, it was concluded that polyether polyol domains do not enter into galleries between the clay layers. For polyol modified epoxy (with no montmorillonite), impact strength showed an increasing trend with increasing polyether polyol contents. However, in the epoxy-montmorillonite binary systems (with no polyether polyol), the impact strength showed a maximum at 1 wt. % montmorillonite content after which, it got reduced. Tensile strength and strain at break showed a maximum at 1 wt. % montmorillonite content in epoxy-montmorillonite binary systems. Finally, it was concluded that in epoxy-montmorillonite-polyether-polyol ternary systems, the impact strength, in general, decreases with respect to increasing amount of montmorillonite. Moreover, the tensile strength and strain at break decreases, in general, as the montmorillonite content increases.

Lam *et al.* (2005) studied the effect of cluster size on hardness of epoxy-clay nanocomposites. Araldite GY 251, HY 956, and SiO_2 were used as epoxy, hardener and nanoclay particles respectively. The mean diameter, density and moisture content of nanoclay were 25 nm, 0.45 g/cm^3 and less than 3 % respectively, with more than 95 % SiO_2. Nanoclay was added into epoxy by mechanical stirring and sonicated at room temperature for 1 h. Hardener was added during mechanical stirring and vacuumed for 24 h. six compositions were fabricated i.e. 0, 2, 4, 6, 10, and 15 wt. %. The hardness increased with increasing clay content and its maximum value obtained was 12.57 Hv for 4 wt. % clay content, which got drastically reduced to 2.68 Hv for 15 wt. % clay content. The diameter of the nanoclay clusters increased with increasing clay content. The average diameter of the clusters measured throughout the whole sample at different locations was about 125 nm for 4 wt. % clay nanocomposite, which got increased to about 400 nm for nanocomposite containing 15 wt. % clay. A long plastic yielding zone was observed for pure epoxy sample in load-extension curve after interlaminar shear strength tests which revealed high fracture energy consumption and toughness of the pure epoxy sample. However, the short beam shear strength of all nanoclay/epoxy composites decreased as compared to neat epoxy sample. The ductility of the 4 wt. % epoxy-clay nanocomposite sample dropped after mixing with nanoclay particles as confirmed by the absence of any plastic yielding zone in load-extension curve. At 15 wt. % clay content, the load-deflection behaviour appeared in a strange way with no possessing of a clear fracture point after the maximum load appeared. Thus, the

microhardness of the 15 wt. % of nanoclay was much lower than the other samples as the deformability of the 15 wt. % of nanoclay was the highest.

Teh *et al.* (2005) fabricated a composite of aromatic epoxy and PET (polyethylene terephthalate fiber) of diameter 20μm and length 2–3mm, 1 wt.% with the objective to investigate the fracture behavior and toughening mechanism of the composite for optimizing the treatment time required for surface modification of PET fibers with NaOH. The morphologies and chemical properties of the as-received composites and the ones with surface modified PET fibers were investigated by SEM and ToF-SIMS (time of flight secondary ion mass spectrometry) techniques. For surface modification, PET fibers were subjected to alkaline hydrolysis with NaOH aqueous solution (50% w/v) at 80℃ for different time periods (0–30 minutes). Subsequently, the samples were washed with distilled water until all NaOH was washed away. ToF-SIMS technique was used to scan the surface topology and internal structure of the PET fibers during hydrolysis (surface modification) before adding them to the epoxy. All fibers were dried at 80℃ for 12 h in vacuum prior to mixing. The composites were prepared by mechanically mixing the short fibers with epoxy resin using a high speed homogenizer (at 700 rpm). Blends were degassed under vacuum and cured at 100℃ for 2 h. The mixture was then poured into a vertical glass mould and post-cured at 180℃ for 5 h. Samples of thickness 6.25 mm and width 12.5 mm (ASTM E 399) were taken for flexural testing (three point bending test) at room temperature. SEM and ToF-SIMS investigations revealed that unmodified fibers showed smooth and featureless surface while the surface of modified fibers appeared with shallow pitting and some cracks for treatment time periods of 2.5 minutes. Fibers treated with NaOH for prolonged time, i.e. 20 minutes resulted in irregular surface and the fibers no longer remained straight. The results also showed that fracture toughness of the neat epoxy increased by 33 % upon addition of 1 wt.% untreated PET fibers and increased by 88 % on addition of 1 wt.% treated (with NaOH for 2.5 minutes) fibers. On increasing the time of surface treatment, toughness decreased because prolonged alkaline hydrolysis led to large accumulation of pits resulting in crack initiation and internal hydrolysis. Fractured surfaces of failed composites were also investigated with SEM. Observations revealed that non-treated fibers showed pullout, leaving clean holes in the epoxy, which represented poor adhesion between fibers and epoxy. The fractured surface of the composite with treated fibers for 2.5 minutes showed typical breakage and river like structures on the surface, which indicated that a lot of energy was utilized during the fracture, while in the sample with treated fibers for a prolonged period (20

minutes treatment time), the river like structure was less apparent, thus concluding that less energy would have been consumed.

Akbari and Bagheri (2007) studied the mechanical properties and deformation mechanism of epoxy-clay nanocomposites. The epoxy, hardener and nanoclay used were Araldite® GY 6010, Aradur 43 BD and NANOLIN DK4 respectively. Organoclay (1.5, 3 and 5 wt. %) was mixed into epoxy at 70 ℃ for 24 h, followed by degassing at same temperature and addition of hardener while mixing for 3 minutes. The samples were cured at room temperature for 24 h and post-cured for 1 h at 100 ℃. XRD analysis showed that the d-spacing of the organoclay increased from 34.23 Å (for pristine clay) to around 44.5 Å (for 5 wt. % organoclay nanocomposite), representing intercalated morphology. It was observed that compressive strength, flexural strength and glass transition temperature (T_g) showed a decreasing trend with increasing clay content, as compared to neat epoxy. Shear bands were observed from the SEM images of failure surfaces of epoxy-5 wt. % montmorillonite nanocomposite under compressive and flexural loading conditions depicted the appearance of shear bands. Although it was expected that organoclay must had increased the yield stress of the nanocomposite system owing to its plasticization effect but the experimental observations illustrated decrement in yield strength with increasing clay loading. The reason reported was the homo-polymerization of epoxy monomers between the clay galleries at high temperature (70 ℃) owing to the catalytic effect of the organo-modifier of the nanoclay. The occurrence of homo-polymerization phenomenon was confirmed by the DSC analysis which showed an another glass transition temperature (around 40 ℃) about 20 ℃ lower than the main transition of the epoxy matrix (around 60 ℃) and it was speculated that this lower T_g belonged to the chains between the silicate galleries. It was reported that when shear stress was applied to such a system, the homo-polymerized epoxy monomers undergo shear deformation easier that the bulk epoxy. The shear deformation, initiated between the clay galleries, propagated into the bulk of material upon further loading and when the shear strain (caused by shear stress) reached the yield strain of the matrix, the material deformed locally and permanently around the layers. Hence, it was concluded that organoclay particles acted as initiation sites for shear bands due to which massive occurrence of shear yielding as well as decrement in mechanical strength was observed. SEM images of pure epoxy was glassy smooth revealing the brittle behaviour of neat epoxy whereas much rougher surface was observed in the nanocomposite containing 5 wt. % MMT. It was also concluded that increased tendency to

shear yield might increase the energy absorption prior to fracture which needed to be confirmed by the fracture toughness and impact strength studies.

Gupta *et al.* (2007) focused on evaluating the effect of the processing method (mechanical mixing and shear mixing) and montmorillonite content on the tensile, compressive and impact properties of clay-epoxy nanocomposites. The ratio of epoxy (D.E.R. 332), diluents (C_{12}-C_{14} aliphaticglycidylether, to reduce epoxy's viscosity) and hardener (amine based D.E.H. 24) was taken as 83.5:4.4:12.1; along with quaternary ammonium salt as clay modifier. Five compositions of nanocomposites, containing nanoclay in 0.125, 0.25, 0.50, 1 and 2 vol. % were taken. Mechanical mixing involved hand mixing; stirring at 650 rpm for 2 hrs; degassing at 45^{o}C; mixing of hardener; curing for 24 h at room temperature and then post curing at 100^{0}C for 3 h. Shear mixed nanocomposites were fabricated in three steps i.e. hand mixing; mixing at 650 rpm for 30 minutes and shear mixing at 180 rpm using three roll mill. Tension and compression tests were performed adopting ASTM D638-02 and ASTM D695-02 specimens while ASTM D4812-05 was for Izod impact testing. TEM analysis shows that mechanical mixed composites do not exhibit any peaks in their spectra while shear mixed shows small bump. The mechanically mixed specimens exhibit a higher modulus than the shear mixed specimens. The effect of nanoclay on the compressive properties of nanocomposites is similar. In case of impact tests, the presence of second phase particles leads to the deflection and branching of the crack tip in composite material and slows down the fracture process, leading to lower slope in the energy-deflection curves. The composites processed by mechanical and shear mixing processes provided exfoliated and intercalated structure, respectively. The tensile and compressive modulus showed improvements with increased nanoclay content. However, the tensile and compressive strengths decreased as nanoclay content increased. The impact strength and energy absorption were higher for mechanically mixed specimens, but lower than the neat epoxy resin. Exfoliated specimens showed better properties than intercalated specimens.

Zaarei *et al.* (2010) studied the impact of organoclay on the physical and mechanical properties of epoxy-clay nanocomposite coatings. The liquid resin, hardener and the nanoclay used in this study were Epon 828, isophoronediamine (IPDA) and organoclay Cloisite 30B respectively. The nanocomposites containing 0, 1, 2, 3 and 4 wt. % nanoclay were formulated by slowly heating DGEBA resin to 50 ℃ and then mixing desired amount of clay while stirring. The mixture was then held at 70–80 ℃ and stirred at 2500 rpm for 2.5 h with a high-shear mixer; followed by degassing in a vacuum oven at 80–85 ℃ for 30 minutes. Then the

clay-resin mixture was sonicated for 150 minutes. and the stoicheiometric amount of hardener was added during a continuous stirring for 3 minutes and sonication for 2 minutes. Finally, the mixture was applied on the pretreated carbon steel plates with a coating film thickness of 27 ± 3 µm and the coating films were post-cured in an oven for 1 h at 100℃. The microhardness, König hardness, abrasion resistance, cupping tests and the impact tests were performed according to ASTM D-1474, ASTM D 4366, ASTM D 4060, BS 3900-part E-4 and ASTM D-5870 respectively. Optical micrographs of uncured specimens showed that the mixing process was efficient for dispersion of the organoclay in the epoxy matrix upto 3 wt. % than at higher concentrations of clay. Dark zones of thick clay sections with the layers tilted to the surface were observed in the TEM of nanocomposite containing 4 wt. % clay suggesting a high level of stacking. The Vickers microhardness of the coatings was enhanced, with the increase in nanoclay content, from 45 to 82 Hv. Also the König hardness of coating films were increased from 131 for neat resin to 145 for 1 wt. % clay and further to 152 for the 4 wt. % clay despite poor dispersion. The result of the cupping test (mm) demonstrated that the increase in the nanoclay loading upto 3 wt. % led to the enhancement of the toughness of the resultant coatings. The results of reverse impact (in.lb) test showed its peak value when the nanoclay content was 2–3 wt. % with a decrease in toughness for the composition containing 4 wt. % clay whereas in direct impact test, all coatings showed relatively high values. Finally, the results of the abrasion test (mg) indicated that the abrasion weight loss of the coatings with high clay loadings was practically negligible, or in other words, the abrasion resistance of the coating was excellent.

Lim and Chow (2011) studied the effects of modified organoclay and its loading on the fracture toughness and morphology of epoxy. The epoxy DGEBA DER 331 (Part A) and curing agent cycloaliphatic amine (Part B) were mixed in the weight ratio 10:6. Prior to mixing, epoxy was degassed for overnight in vacuum oven while OMMT was dried at 100 ℃ for 12 h in a conventional oven, followed by mixing of OMMT (1–5 wt. %) in Part B while stirring at 1000 rpm for 1 h. The Part B/OMMT mixture was then added to Part A while stirring at 100 rpm for 5 minutes; pouring the mixture into the mold; degasification in vacuum oven for 25 minutes at 35 ℃ and finally curing in an oven at 100 ℃ for 1 h. XRD analysis showed that the *d*-spacing for OMMT is 2.14 nm whereas for epoxy-OMMT nanocomposites, no intense diffraction peak was observed in the range of $2\theta = 2^{o}–10^{o}$, indicating the disappearance of clay ordered structure. However it was also observed that for 5 wt. % clay nanocomposite, a little diffraction peak was observed which showed that the

OMMT platelets were not fully exfoliated but contained a little amount of tactoids or clay ordered structures in the matrix. The addition of organoclay was found to increase the plain strain/ critical intensity factor (K_{IC}). The inclusion of OMMT increased the fracture toughness of the neat epoxy resin by almost 80 % with only 5 wt. % clay. The results of FESEM showed that there were organoclay tactoids present in the highly filled nanocomposites. Surprisingly, the aggregates also acted as an obstruction to block the growing crack front and resulted in higher degree of crack deflection.

Mouloud *et al.* (2012) studied the effect of addition of three different types of montmorillonite clays on the morphological and mechanical properties of epoxy based nanocomposites. Two of these were commercially available clays (72T and 67G) and the third type was a laboratory preparation (BNTC18). The samples were prepared by mixing of epoxy and clay in the requisite amounts and hand-stirring for 2h; immersion of mixture in water bath at 40℃ with mechanical stirring at 1000 rpm; amine hardner addition and mechanical stirring for 1h at 40℃; degassing under vacuum for a few minutes and pouring in aluminum mould; curing for 24 h in ambient conditions and post-curing at 130℃ for 3h. Impact strength tests were performed according to ASTM D256–97 while for fracture toughness ASTM E399–06$^{\varepsilon 2}$ standard was used. For both 72T and 67G, XRD analysis showed intercalation of polymer into clay galleries for 4 phr clay content while for BNTC18, a disordered intercalate morphology for 2 phr clay was observed. The T_g showed a decreasing trend for 72T and 67G with increasing clay content while for BNTC18, T_g showed minimum value at 2 phr clay content and an increasing trend afterwards. Elastic modulus increased with increasing the clay content and higher values were observed in case of BNTC18. For young's modulus, Clays 72T and 67G were found to have different response than BNTC18 because dimethyl dihydrogenated modifier was used in both of them whereas octadecylammonium was used in BNTC18. The impact strength showed an increase till 2 phr after which it showed a decreasing trend in all the three cases. The fracture toughness showed its maximum value at 2 phr clay content after which it decreased and got leveled off in all the cases. The epoxy/clay composites with intercalated structure were obtained. The addition of organically modified nanoclay platelets according to operative conditions and processing used here (mechanical stirring) improved mechanical performances at low clay concentration (optimal content around 2 phr).

Ngo *et al.* (2012) studied the effect of dispersion and intercalation/exfoliation of organoclay (2 wt. %) on the mechanical properties of epoxy nanocomposites. The epoxy used was

standard DGEBA resin (EPON^{TM} Resin 828); hardener was Jeffamine® D-230; organoclay was Cloisite® 30B and clay modifier was quaternary ammonium. Epoxy and clay were mixed together in six conditions i.e. 'room temperature without mechanical shear (Rm)', 'high temperature without shear (Tm)', 'high temperature and low-speed mixing (TM)', 'room temperature and high-speed mixing (RS)', 'high temperature and high-speed mixing' and 'high-pressure process (HP)' and samples were fabricated according to ASTM D638−2002 and ASTM D695-2002 standards for tensile and compressive tests. The epoxy system and its nanocomposites were cured at 120 ℃ for 2h, with subsequent post-cure at 140 ℃ for 2h. The XRD analysis showed that the peak positions of the epoxy nanocomposites were different depending on the pre-mixing methods. According to the intensity and position of the XRD peaks, the orders of intercalation/exfoliation can be ranged as TS > HP ~ RS, TM > Tm > Rm, TS > TM > Tm and RS > Rm. This study demonstrated that even with a small amount of clay (2 wt %), the tensile modulus can be significantly improved and it follows the pattern $E_{TS} > E_{HP} > E_{RS} > E_{TM} > E_{Tm} > E_{Rm} > E_{Epoxy}$. Similar trend was seen for the tensile strength. Compressive tests also gave the same results. The storage modulus in the both glassy and rubbery regions is generally higher for the nanocomposite samples than for the neat epoxy system. However, the level of increase in modulus in the rubbery region is higher than in the glassy region. Tensile modulus and strength of epoxy nanocomposites containing different clay concentrations and prepared with high speed at high temperatures (TS) or at high temperature without mechanical stirring (Tm) showed a linear increase. Similar results were seen for compressive properties.

Olad *et al.* (2012) investigated the mechanical and thermal properties of intercalated epoxy/layered silicate nanocomposites. The epoxy and hardener user were Epiran-05 and EPIKURE curing agent 3200, Aminoethylpiperazine (AEP) respectively. Organically modified clays used were Cloisite 30B (d-spacing = 18.5 Å) and Cloisite 15A (d-spacing = 29.88 Å) along with a K-10 grade MMT. Both tetraethylammonium chloride (TEA) and the selected curing agent were used as an intercalating agent of unmodified MMT. The inorganic Na-MMT was modified with AEP and TEA by carrying out the cation exchange process between MMT and intercalating agents. The DGEBA resin was vigorously stirred with different amounts of clay powders (modified and unmodified) at 50 ℃ and 6 h, followed by ultrasonication in an ultrasonic bath. Hardener was added, mixture was degassed in vacuum over for 15 minutes and finally curing was performed for 24 h at 40 ℃. FTIR spectroscopy confirmed the organic modification of MMT by chloride salt of TEA and AEP amine

intercalating agents. After XRD, the d-spacing of Na-MMT, TEA-modified MMT and AEP-modified MMT was obtained 12.38 Å, 14.52 Å, and 15.58 Å respectively. The XRD patterns for epoxy-clay nanocomposite with Na-MMT, TEA-modified MMT, AEP-modified MMT, was obtained 16.74 Å, 17.90 Å, and 18.33 Å respectively whereas for both Cloisite 15A and Cloisite 30B, it was ≈ 31.6 Å due to which it was concluded that the highest increase in the d-spacing was obtained or epoxy/Cloisite 30B nanocomposite. The adhesion strength (ASTM D3359-83) was found maximum for all compositions of epoxy/Cloisite 30B nanocomposite (1, 3, and 5 wt. % nanoclay). The Shore D hardness (ASTM D-2240) was observed to increase with increasing clay content for all types of clays. For epoxy/Cloisite 30B nanocomposite system, the tensile strength and elongation at break were lower than that of the neat epoxy and they decreased with increasing clay content, whereas modulus showed an increasing trend (ASTM D-638). DSC analysis showed that the glass transition temperature (T_g) of the composite system got enhanced to 125.3 ℃ for 5 wt. % epoxy-clay nanocomposite, compared to 70 ℃ for neat epoxy. TGA analysis showed that the T_d (the temperature of degradation at which weight loss is 20 %) of 3 wt. % epoxy/Cloisite 30B composite system was shifted to 319 ℃, compared to 313 ℃ for pure epoxy sample. SEM analysis of fractured surface of pure epoxy showed that it is quite smooth revealing brittle fracture behaviour whereas it was observed to be rough for 3 wt. % epoxy/Cloisite 30B nanocomposite system.

Kusmono *et al.* (2013) studied the effect of clay addition on the mechanical properties of epoxy/clay nanocomposites through tensile, flexural, impact strength, and fracture toughness tests. The epoxy resin used was DGEBA DER 331; polyaminoamide as curing agent/hardener and montmorillonite clay as the reinforcement. The procedure followed for nanocomposite fabrication was pre-heating the clay at 80 ℃ for 8 h; mixing clay and epoxy resin at 0, 2, 3, 4, 5 and 6 wt. % of clay at 75 ℃ for 2 h using mechanical stirrer; degassing for 15 minutes; addition of curing agent at 75 ℃ for 5 minutes; again degassing for 3 minutes, pouring into steel mold, again degassing for 10 minutes; curing at 80 ℃ for 2 h and finally post-curing at 150 ℃ for 2 h. ASTM D638 M standard was used for tensile tests, ASTM D790 for flexural strength tests, ASTM 256–02 for impact tests and ASTM D5045–96 for measuring fracture toughness. XRD analysis showed the absence of any peak in case of 3 wt. % epoxy/clay nanocomposites which showed the formation of exfoliated structure. The maximum tensile strength, flexural strength, impact strength and fracture toughness was observed at 3 wt. % clay due to exfoliated structure after which, it got reduced due to

agglomeration of clay particles, which failed to provide a torturous path against crack propagation and even acted as initial cracks. High clay loading showed an improvement in specific abrasion. SEM analysis showed increased roughness of the fracture surfaces for 3 wt. % nanocomposites, as compared to neat epoxy. The tensile strength, flexural strength, impact strength, fracture toughness and specific abrasion showed 41, 20, 95 and 19% improvement compared to neat epoxy.

Bashar *et al.* (2014) studied the effect of nanocomposite structure on fracture behaviour of epoxy-clay nanocomposites prepared by different dispersion methods. The epoxy and hardener used were EPON 826 and EPIKURE 9551 whereas the organoclays used were Nanomer I.28E (d-spacing = 2.39 nm) and Nanomer I.30E (d-spacing = 2.23 nm) alongwith an unmodified PGW sodium MMT (d-spacing = 1.24 nm) nanoclay. Two processing methods were selected i.e. mechanical dispersion and ultrasonic dispersion. In mechanical mixing, preheated Nanomer I.30E (120 ℃ for 24 h) was added to EPON 826 (preheated at 60 ℃) and mechanically mixed for 30 minutes at 900 rpm. Stoichiometric amount of curing agent was added to epoxy-clay solution during mechanical mixing at 60 ℃ for 5 minutes, followed by degassing and finally curing in steel moulds at 120 ℃ for 2 h. In ultrasonic mixing method, dried clay was added into acetone, followed by holding the mixture at room temperature for 6 h. The solution was then added into EPON 826 (preheated at 60 ℃) and subsequently sonicated at 80 ℃ for 8 h, followed by mechanical blending for 2 h. Acetone was removed by vacuum extraction performed at 80 kPa and finally, hardener was added and mechanically mixed for 30 minutes at 900 rpm. Nanocomposites containing 1, 2, and 3 wt. % I.30E were fabricated by both methods whereas 1 wt. % I.28E nanocomposite and 1 wt. % PGW nanocomposite were only fabricated with ultrasonic dispersion. From the XRD of the specimens prepared from ultrasonic dispersion, it was observed that 1 and 2 wt. % I.30E nanocomposites showed complete exfoliation whereas the d-spacing of 3 wt. % I.30E nanocomposites was increased to 2.73 nm. The nanocomposites containing 1 and 3 wt. % I.28E, prepared by mechanical mixing, showed the d-spacing as 2.68 nm and 2.63 nm respectively. The d-spacing for 1 wt. % I.28E and PGW nanocomposites was obtained 2.39 nm and 1.24 nm, showing intercalated and phase-separated morphologies respectively. The tensile modulus and strength of neat epoxy was measured to be 2.8 GPa and 82 MPa respectively whereas 20 % improvement in tensile modulus was obtained in response to 3 wt. % I.30E nanoclay addition. But for the mechanically mixed samples, the modulus increase was very small owing to the insufficient layer separation of the nanoclay. Tensile strength

values remained almost unchanged for samples formulated by ultrasonic mixing whereas nanocomposites made my mechanical mixing method exhibited a considerable loss in tensile strength. The fracture toughness of the neat epoxy was measured as 0.78 MPa√m. for ultrasonically produced nanocomposites, the toughness value remained almost identical to that of the pristine epoxy. However, the fracture toughness increased substantially for the mechanical dispersion method, for example, by mechanically mixing 3 wt. % of I.30E clay with epoxy, an increase of about 35 % was observed relative to unmodified epoxy. SEM fractographic analysis showed that neat epoxy exhibited smooth and featureless fracture surface revealing brittle type fracture behaviour. The fracture surface of ultrasonically mixed I.30E clay nanocomposite was coarse and rough, indicating role of crack deflection mechanism whereas for mechanically mixed I.30E clay nanocomposite, both crack deflection and crack pinning mechanisms played a big role in increasing absorbed energy before fracture. Fracture surface analysis of I.28E clay nanocomposites revealed crack deflection, crack pinning mechanisms, alongwith localized matrix deformation.

Raturi (2014) studied the mechanical and morphological properties of an epoxy-clay-PET nanocomposite system. The nanoclay (Cloisite 15A) was added into the epoxy resin (Araldite GY 257). The mixture was homogenized at 20,000 rpm for 10 minutes, followed by probe sonication at 50 amplitude for 10 minutes. Curing agent (Araldite HY 837) was added into this mixture in a 100:35 weight ratio, along with the addition of PET fibers, during mechanical stirring at 500 rpm for 10 minutes. The alkaline surface treatment of the PET fibers was performed using 50 % w/v NaOH solution at 31, 50 and, 80 ℃ for 2.5, 5, 10, 15, 30 and, 45 minutes. Nine run orders constituting different wt. % of epoxy (96.25–100 wt. %), clay (0–2.25 wt. %) and PET (0–1.5 wt. %) were obtained from the mixture design module of Minitab 17. The tensile tests were performed according to the ASTM D3039/3039M standard whereas the flexural tests were performed according to ASTM D790 standard. XRD analysis showed that the d-spacing of clay increased from 19.96 Å (pristine clay) to a higher range of 29.2–30 Å (for 1.5 wt. % clay loading). The maximum tensile strength obtained was recorded 41.9 MPa for 1.5 wt. % PET and 0 wt. % clay nanocomposite system. Nanocomposites containing both PET and clay in their higher ranges deteriorated the tensile strength considerably but the clay present alone, even at its maximum 2.25 wt. %, did not deteriorated the tensile strength considerably. Addition of fillers (either clay, or PET or both) lowered the flexural strength with reference to that of the neat epoxy-hardener system (93.7 MPa). The maximum flexural strength observed for the nanocomposite system was 83.3 MPa for 2.25

wt. % clay and 0 wt. % PET. Similar to the tensile strength, it was observed that when both the fillers were present in their higher ranges, the flexural strength values dropped drastically. The maximum improvement in the flexural modulus was observed for epoxy-clay blend containing maximum weight percentage of clay (2.25 wt. %) and its value was 3500 MPa, which showed a 10 % improvement as compared to the base material. Mixture contour plot, mixture surface plot and cox response trace plot for tensile and flexural properties, obtained from the mixture design module of Minitab 17, were in agreement with the obtained experimental results. SEM image analysis for the composite systems containing treated fibers showed that at the treatment temperature 31 ℃, the surface of PET fibers was not modified adequately to facilitate any increased adhesion of PET to the resin. Also, for the treatment temperature 50 ℃ and treatment time 15 minutes, SEM images showed a non-uniform disfigurement over the fiber surfaces. However, significant amount of delusturing and pitting was noticed at treatment temperature 80 ℃ , for treatment times 2.5, 5, 10, 15 minutes. Finally, maintaining the temperature as 80 ℃ and increasing the treatment time to 30 minutes and 45 minutes, scaling-off of the edges of the fibers, formation of small craters/pores and excessive bending of the fibers were observed. The optimum alkaline treatment temperature selected from the SEM image analysis was 80 ℃. PET fibers were alkaline treated at this temperature for 2.5, 5, 10, 15 minutes and, nanocomposite were fabricated from it, using the composition 0.8 wt. % clay and 1 wt. % PET. However, the best tensile strength result was obtained with 15 minutes treatment time i.e. 44.5 MPa. Hence, corresponding to this treatment temperature and time, flexural tests was performed which showed a slight decrease in the nanocomposite's flexural modulus (from 2277.5 MPa for untreated fiber to 1943.333 MPa for 15 minutes treatment time). Moreover, the bending strength changed from 66.25 MPa for untreated fibers to 65.5 MPa for 15 minutes treatment time.

Sharmila *et al.* (2014) fabricated partially exfoliated and disordered intercalated Cloisite epoxy nanocomposites via *in situ* polymerization and studied their mechanical, thermal and barrier properties. The epoxy, hardener and clay used were Araldite GY 250, HY 951 and Cloisite 93A respectively. Cloisite epoxy nanocomposites (CPNs) were fabricated by mixing 0–5 phr clay into epoxy prepolymer during mechanical stirring for 45 minutes and sonication for another 30 minutes. Then, 10 phr hardener was added, followed by 5 minutes of mixing and degassing. The samples were cured at room temperature for 24 h and post-cured at 80 ℃ for 4 h. XRD analysis showed that the d-spacing for pristine clay was 2.372 nm but no diffraction peak was observed for EC0 and EC0.5 nanocomposites, indicating some extent of

exfoliation. However, EC5 nanocomposite showed the 001 diffraction peak corresponding to d-spacing of 3.242 nm indicating intercalation. TEM images showed that both intercalated and exfoliated structures were present in EP1 nanocomposite, designating it as partially exfoliated/disordered intercalated morphology whereas EP5 nanocomposite depicted formation of aggregates and thicker Cloisite particles, confirming the presence of intercalated structure. The tensile strength and flexural strength of neat epoxy was found to be 54 MPa and 64 MPa respectively. However, upon addition of 1 phr clay, 15 % increase in tensile strength, 23 % increment in flexural strength and 19 % increment in elastic modulus were obtained whereas strain at break (%) values decreased with increasing clay content, as compared to neat epoxy. CPN at 1 phr Cloisite loading showed an enhancement of 37 % in hardness compared to pure epoxy. SEM fractography showed that neat epoxy resin exhibited smooth fracture surface with occasional river patterns representing brittle failure whereas upon addition of clay, the fracture surface became rough and mechanisms like crack deflection, crack pinning and crack arresting came into action. Swelling tests results showed that the barrier performance of CPN increased to a greater extent compared to the neat epoxy. There were 50, 61 and 45 % increase in barrier performance upon addition of 5 phr nanoclay, compared to neat epoxy, in acidic, aqueous and basic medium respectively. Moreover, the mass uptake in acidic medium was higher than that in aqueous and basic medium. Cross link density (CLD) of the pure epoxy increased from 13.6×10^{-3} g mol cm^{-3} to 15.12 g mol cm^{-3} upon addition of 1 phr nanoclay, followed by a decreasing trend in CLD due to plasticization effect imparted by clay at its higher loading values. TGA analysis showed that the onset thermal degradation temperature (T_0) and (T_{80}) (temperature for 80 % mass loss) increased significantly with increasing Cloisite content, which represented improved thermal stability of CPNs, whereas T_{max} (temperature for maximum mass loss) and T_{10} (temperature for 10 % mass loss) remained almost unaltered. Enhancement of 14^o and 20^o in T_0 and T_{80} at 5 phr clay loading, as compared to neat epoxy, indicated improved thermal stability.

Sánchez-Cabezudo *et al.* (2015) studied the morphology and mechanical properties of epoxy/thermoplastic/organoclay systems. The epoxy, hardener and thermoplastic used were DGEBA Araldit F, 4,4'-diamino diphenylmethane (DDM) and poly (vinyl acetate) (PVAc) respectively whereas, the nanoclays used were Cloisite 30B (C30B) and Cloisite 93A (C93A). DGEBA-PVAc mixtures were prepared by dissolving PVAc in DGEBA at 90 ℃ using magnetic stirrer for 4 h. Nanoclay powders were added into the obtained mixtures and stirred at 300 rpm at 90 ℃ for 18 h, followed by degassing for 1–2 h at 120 ℃. Finally, curing

agent was melted and mixed at 100 ℃ while stirring for 5 minutes. The composites were cured at 120 ℃ for 2 h and 180 ℃ for 30 minutes. The clay content was maintained as 4 wt. % whereas PVAc was varied between 0–20 wt. %. DSC analysis showed that the T_g of the neat epoxy (–15 ℃) increased with the addition of organoclays (–12 ℃ and –11 ℃ for C30B and C93A, respectively) alongwith the increased T_g of C30B and C93A dispersions in DGEBA-DDM/PVAc mixture, with rising PVAc content. WAXS results showed that the d-spacing of C30B and C93A was 1.85 nm and 2.36 nm respectively whereas the d-spacing of epoxy/C30B nanocomposite and epoxy/93A nanocomposite was obtained 3.38 nm and 3.30 nm respectively which showed that epoxy molecules intercalated better in C30B than in C93A. However, upon incorporation of PVAc, only very small increase in d-spacing was observed which showed that the addition of PVAc not modified the intercalated morphology. SEM micrographs of epoxy/5 wt. % PVAc showed that PVAc formed an immiscible phase in the epoxy matrix, giving rise to spherical domains whereas in ternary nanocomposites, clay aggregates were also visible. The diameters of the PVAc domains were 100–200 nm in the samples having no clay and 100–400 nm in the ternary nanocomposites. SEM of epoxy/10 wt. % PVAc/C93A and epoxy/15 wt. % PVAc/C93A illustrated the combined morphology of nodular regions (PVAc spheres in epoxy matrix) and inverted regions (epoxy spheres surrounded by PVAc) held together by fibrils and indicated some interpenetration of PVAc and epoxy at the interfaces. But the SEM micrographs of epoxy/20 wt. % PVAc/C30B and epoxy/20 wt. % PVAc/C93A composites revealed epoxy spheres surrounded by the thermoplastic-phase whereas the undetected clay was suggested to be located inside the epoxy spheres. TEM micrographs of epoxy/C30B and epoxy/C93A nanocomposites showed clay tactoids with interplatelet spacing in agreement with WAXS results. Also, the TEM micrographs of ternary nanocomposites illustrated that for samples containing 5 wt. % PVAc , clay tactoids and 100–400 nm PVAc domains were observed to be dispersed in the epoxy matrix, in agreement with SEM results whereas, the samples containing 20 wt. % PVAc showed clay tactoids dispersed in epoxy phase and epoxy formed spheres in the matrix of PVAc as it corresponded to an inverted morphology. The tensile modulus of neat epoxy was observed to be (2.5 ± 0.2 GPa), which got increased to 3.0 ± 0.2 GPa and 2.8 ± 0.2 GPa for C30B and C93A respectively but showed a decreasing trend with increasing PVAc content (and 0 wt. % clay). The tensile modulus of the epoxy/PVAc/C30B and epoxy/PVAc/93A were higher than that of the epoxy/PVAc blends, showing increments of 20–36 % with C30B and 12–32 % with C93A, signifying the reinforcing action of the clay. The tensile strength

values hardly changed with C30B (65 ± 4 MPa) loading and showed a decrease with C93A loading (54 ± 3 MPa), as compared to neat epoxy (63 ± 4 MPa), but it showed a decreasing trend with increasing PVAc content (and 0 wt. % clay). Moreover, the decrease in tensile strength of epoxy/PVAc/C93A nanocomposites suggested that the interfacial strength between the organoclay and the matrix was weaker than in epoxy/PVAc/C30B nanocomposites. The strain at break value and estimated toughness from the tensile curve, for neat epoxy, was observed to be 3.7 ± 0.7 % and 137 ± 35 MJ/m^3 respectively, which got improved upto 60 and 70 % respectively upon addition of 10 wt. % PVAc. The addition of clays to the epoxy and to epoxy/PVAc blends led to a reduction of the strain at break and toughness which was slightly greater for C93A nanocomposites. The epoxy/5 wt. % PVAc/C30B and epoxy/5 wt. % PVAc/C93A nanocomposites exhibited lower strain at break and toughness than neat epoxy thermoset but epoxy/10 wt. % PVAc/C30B and epoxy/10 wt. % PVAc/C93A exhibited higher strain at break and toughness than neat epoxy thermoset.

Ying *et al.* (2015) studied the mechanism of exfoliation and thermal/mechanical properties of highly exfoliated epoxy/clay nanocomposites. The epoxy and nanoclay used were EPON 828, and Cloisite Na^+ respectively whereas the hardeners were DMP-30 and J230. 10 g pristine clay was dispersed into 1500 ml of distilled water at 80 ℃. 60 ml of 0.24 N HCl solution and 4.2 g of DMP-30 were added into 100 ml distilled water during magnetic stirring to obtain Protonated form of DMP-30. The obtained solution was added into hot clay/water suspension during vigorous stirring for 8 h at 80 ℃ for obtaining a pale yellow precipitate. This modified clay (M-clay) was filtered and washed with acetone, followed by the addition of acetone/M-clay slurry into epoxy, while stirring at 80 ℃ for 2 h. When the mixture got cooled down to 50 ℃, stoichiometric amount of J230 was added and blended for 10 minutes using a magnetic stirrer., followed by degassing at 60 ℃ and curing at 75 ℃ for 2 h while post-curing at 120 ℃ for 8 h. TEM analysis showed that the clay particles were uniformly dispersed in the epoxy matrix without any presence of large agglomerates. Clay platelets had been exfoliated disorderly in the form of very thin tactoids consisting of a single platelet or 2–3 layers of clay. XRD diffractograms showed that the pristine clay and, and M-clay washed with water showed peaks at $2\theta = 8^o$ and 6^o, respectively. The acetone washed M-clay exhibited the same peak as that for M-clay washed with water. However upon its addition into epoxy prepolymer, a very weak peak was observed indicating exfoliation of clay layers prior to curing. But epoxy/M-clay nanocomposite containing 3 wt. % clay showed no diffraction peak indicating disorderly and highly exfoliated epoxy/clay nanocomposite system. DSC analysis

showed that the T_g of the neat epoxy (85.5 ℃) increased with increasing clay content and its values for 1 wt. %, 2 wt. %, and 3 wt. % clay nanocomposites were obtained as 92 ℃, 93.5 ℃ and 95.5 ℃ respectively. Flexural properties of pure epoxy and epoxy-clay nanocomposites, studied at room temperature, showed that the flexural strength of epoxy-clay nanocomposites decreased marginally compared to neat epoxy, attributed to the presence of air bubbles entrapped during fabrication whereas flexural modulus of the nanocomposites increased substantially with increasing M-clay contents. However, flexural properties of pure epoxy and epoxy-clay nanocomposites, studied at 80 ℃, showed that the flexural strength of epoxy-clay nanocomposites significantly increased with increased M-clay content upto ~ 2 wt. %, followed by a decreasing trend whereas the flexural modulus showed the similar trend as that for room temperature studied composites and nanocomposites. Also it was noted that at 80 ℃, the flexural modulus of the neat epoxy dropped from 2.8 GPa (at room temperature) to 1.85 ℃.

2.3 Summary of the Reviewed Literature

- Several authors have reported improvement in mechanical properties (tensile strength, tensile modulus, flexural strength, flexural modulus, impact strength, fracture toughness and microhardness) with the addition of nanoclay [Yasmin *et al.,* 2003; Isik *et al.,* 2003; Lam *et al.,* 2005; Akbari and Bagheri, 2007; Gupta *et al.,* 2007; Lim and Chow, 2011; Mouloud *et al.,* 2012; Ngo *et al.,* 2012; Olad *et al.,* 2012; Kusmono *et al.,* 2013; Bashar *et al.,* 2014; Raturi, 2014; Sharmila *et al.,* 2014; Sánchez-Cabezudo *et al.,* 2015; Ying *et al.,* 2015].
- Some authors have studied the effect of nanoclay addition on the thermal properties (weight loss % and T_g) of epoxy-clay nanocomposite systems [Isik *et al.,* 2003; Mouloud *et al.,* 2012; Olad *et al.,* 2012; Sharmila *et al.,* 2014; Sánchez-Cabezudo *et al.,* 2015; Ying *et al.,* 2015].
- Some authors have incorporated different modified and unmodified clays (having different d-spacings, as confirmed by XRD) and studied relative effect on the properties of the nanocomposite systems fabricated [Mouloud *et al.,* 2012; Olad *et al.,* 2012; Bashar *et al.,* 2014; Sánchez-Cabezudo *et al.,* 2015].
- Some authors have fabricated nanocomposite systems using different processing methods (3-roll milling, mechanical mixing, shear mixing, ultrasonication etc.) and studied their

relative effects on the properties [Yasmin *et al.*, 2003; Gupta *et al.*, 2007; Ngo *et al.*, 2012; Bashar *et al.*, 2014].

- A few authors have studied the effect of reinforcing the polymeric thermoset matrix with polymeric fibers, for example, polyethylene terephthalate (PET) fibers [Teh *et al.*, 2005; Raturi, 2014].
- Some authors have studied the trends followed by different properties of epoxy-clay nanocomposites upon incorporation of a tertiary reinforcement like polyether polyol, polyethersulphone, poly (vinyl acetate) etc. [Isik *et al.*, 2003; Sánchez-Cabezudo *et al.*, 2015].
- Some authors have worked in the area of barrier properties of epoxy-clay nanocomposites [Kusmono *et al.*, 2013; Sharmila *et al.*, 2014;].

2.4 Gaps in the Reviewed Literature

- Very limited literature has been reported on the effect of nanoclay addition over the tribological properties of epoxy-clay nanocomposites.
- More studies are required to be performed in the area of barrier properties (solvent uptake) of epoxy-clay nanocomposites.
- There is still a need of extensive research in the area of trend followed by the mechanical properties of epoxy-clay nanocomposites upon reinforcement of PET fibers.
- Different researchers have used different degassing periods but reason for selecting a particular time period and calculations regarding it have not been discussed.
- Dispersion of clay takes place during premixing (before curing). Different methods (varying the shear rate and temperature) have been studied by various authors to achieve fine dispersion and complete exfoliation, but still 100% complete exfoliation has not been achieved which means that there is still a scope of work to develop finer dispersion and well-exfoliated morphologies.

Chapter 3
Design of the Study

3.1 Introduction

This chapter describes the design of the proposed work. It includes the overall objective of the proposed work, the research methodology, basic information regarding constituents of the prepared nanocomposites. It also covers details of equipment and instruments used in conduct of the experimental work.

3.2 Scope of the Study

The scope and requirement for this study can be well explained by understanding the application areas of epoxy-clay nanocomposites as discuss as follows:

1. Epoxy resins have been widely used as encapsulating materials for electronic devices. However, the epoxy resins are not necessarily satisfactory in such applications where a high degree of heat resistance, adhesion, dimensional stability, or less hygroscopicity is required. This has significantly restricted their use in molding or packaging applications. Therefore, an improvement upon epoxy encapsulating materials is called for. But, the addition of clay greatly improves the adhesion and lowers the hygroscopic characteristic so that they become highly suitable for practical use as encapsulating materials for electronic devices [Tsai *et al.*, 2003].
2. Epoxy resins are widely used as matrices in advanced composites due to their good impregnation and adhesion to fiber reinforcement, resulting in excellent mechanical performance; chemical and electrical resistance and low shrinkage on cure. Their use is, in particular, justified in application areas where their technical advantages balance their relatively higher costs compared to other thermosetting polymers e.g. in aviation industry. However, flammability of epoxy resins still represents a limitation in structural applications as an incidental fire event involves not only health risks, but also loss of mechanical properties. In order to meet application requirements, their flame retardant properties have to be improved while maintenance of other important characteristics such as mechanical and thermal properties [Toldy *et al.*, 2011]. MMT frequently exhibits unexpected properties including reducing gas permeability, improved solvent resistance, and superior mechanical and enhanced flame retardant properties [Rashmi *et al.*, 2011].

3. Nowadays, commercial aircrafts are equipped with fuel tanks that are principally situated in their wings. These tanks, known as integral fuel tanks, are formed by the actual structure of aircraft and contain large amounts of jet fuel. The use of integral fuel tanks is preferable in the aerospace industry since they utilize the primary structure, which is already designed to sustain loads. They demonstrate major advantages over rigid removable and bladder fuel tanks as they have a greater capacity and additionally they do not add more weight to the aircraft. However, the design of an integral fuel tank presumes the use of suitable materials that will provide and ensures a good seal of the structure throughout its service life. Fuel tank sealants are applied between faces of assemblies (interfay sealants), used for filleting (fillet sealants) and applied over rivers (overcoat sealants) to achieve the best seal for the wing structure. Due to the extreme environment, that they are exposed to and the combination of loads and elements such as water/fuel presence in addition to very low temperatures, a number of tests should be performed to characterize and qualify a sealant material. Therefore, mechanical and physical testing is performed under various conditions to ensure that the materials are fit for purpose [Giannis *et al.,* 2008].
4. Recently many attempts were made to develop epoxy resin composites modified by nanofillers to improve the mechanical and tribological performance of the epoxy matrix. Moreover, in the context of applications as a bearing material (journal bearings and sliding components) in automobiles, the performance of MMT filled epoxy nanocomposite is good and possibly superior to neat epoxy [Rashmi *et al.,* 2011].

All the above mentioned applications show that there is a lot of scope for research for enhancing the mechanical performance of epoxy-clay nanocomposite systems, which has led to the origin of this study.

3.3 Establishing the Objective Function

The main emphasis of present study is to evaluate the mechanical properties (tensile, impact and microhardness) of the epoxy-hardener system reinforced with a silicate nano-filler. In the present work, MMT clay has been utilized as the nano-filler. The overall objective of the present work is to evaluate **the effect of MMT clay addition on the mechanical performance of epoxy based PMNC system.** The key issues that have been taken up during this study include the fabrication of nanocomposites with different concentration levels of nano-fillers and their subsequent evaluation for mechanical performance (tensile, impact, and

microhardness testing). The trends followed by different mechanical properties arising due to the effect of nanoclay addition have been studied. The present study also involves the characterization procedures viz XRD and SEM analysis. XRD analysis has been done to study the level of intercalation/exfoliation of the epoxy resin between the clay galleries (distribution of the secondary phase) for a given clay loading. SEM analysis has been conducted to determine the deformation and failure mechanism involved during tensile and impact testing respectively.

3.4 Research Methodology

This section presents the detailed procedure to be followed during the fabrication, characterization and testing of the nanocomposite systems. The research methodology followed is aimed to determine the concentration levels of nano-fillers in the proposed nanocomposite systems. It commences with the review of literature for gaining information regarding the range of the concentration (wt. %) of clay to be used, followed by the characterization and evaluation of mechanical properties (tensile, impact and microhardness testing) of the resulting nanocomposites. The general methodology adopted in the present dissertation work comprises of the following steps:

- The nanoclay is dispersed into the epoxy matrix by using homogenization and probe sonication procedures.
- The hardener is added to the epoxy-clay system, followed by pouring the formulated resin-clay system into aluminium moulds and test tubes.
- The formulated nanocomposites are characterized using XRD (study the level of intercalation/exfoliation) and SEM (study the failure mode from fractured surfaces).
- Samples for mechanical testing are generated and tested to study the effect on nanoclay over the properties.

3.5 Material Selection

This section deals with the various constituents selected for the fabrication of nanocomposite system.

3.5.1 Epoxy Resin

The epoxy resin investigated in the present work is a combination of epoxy and the hardener, both belonging to *Araldite family*. The epoxy used is *Araldite® GY 257 IN* and the hardener is

Aradur 837; supplied by *Huntsman Advanced Materials, India*. It has good mechanical properties and chemical resistance; variable within wide limits by using changing hardeners and fillers. It also shows good processing properties. It has a density of 1.15 g/cm^3 at 20 ℃ and a viscosity of 500–650 mPa-s at 25 ℃. The resin system and hardener are mixed in 100:35 weight ratios (as specified by the supplier).

3.5.2 MMT Clay

The MMT clay used is the *Cloisite® 93A*, which is a natural montmorillonite used as an additive for plastics to improve various properties, such as reinforcement, HDT, CLTE and barrier properties. This clay (*Supplier: NANOSHEL LLC, Wilmington DE, USA*) has an average particle size < 80 nm, purity > 99%, along with the density 2.86 g/cm^3 and hardness 5.5 on Mohs scale. It also has pH value 8–9, specific surface area (BET) 50–70 m^{2}g and softening temperature as 980 ℃ [Web Reference: http://www.nanoshel.com/product/cloisite-93a-montmorillonite-nano-powderspurity-99-aps/].

3.6 Input Parameters

This section describes the various input parameters for the fabricated nanocomposite system and selected levels of concentration of constituents.

3.6.1 Concentration of MMT Clay and Epoxy Resin

The concentration of the MMT clay is selected in the range 0–4 wt. % through a detailed literature review [Isik *et al.,* 2003; Yasmin *et al.,* 2003; Liu *et al.,* 2004; Basara *et al.,* 2005; Lam *et al.,* 2005; Wang *et al.,* 2005; Mohan *et al.,* 2006; Khanbabaei *et al.,* 2007; Zaarei *et al.,* 2010; Lingaraju *et al.,* 2011; Bakar *et al.,* 2012; Mouloud *et al.,* 2012; Ngo *et al.,* 2012; Kusmono *et al.,* 2013; Al-Qadhi *et al.,* 2013; Bashar *et al.,* 2014; Al-Qadhi *et al.,* 2014; Sharmila *et al.,* 2014]. The maximum limit has been selected as 4 wt. % because above this value many authors have reported either deterioration of mechanical properties or improvement in mechanical properties is quite less owing to the possible agglomeration of clay particles due to high clay content. In accordance with the clay content selected, the epoxy resin has been varied in the range 96–100 wt. %. Table 3.1 shows the clay loading values selected for investigating the performance of nanocomposites.

Table 3.1: Concentration of nanoclay in different nanocomposite formulations

Sample No.	Clay loading (wt. %)	Epoxy resin content (wt. %)
1	0.0	100.0
2	0.5	99.5
3	1.0	99.0
4	1.5	98.5
5	2.0	98.0
6	3.0	97.0
7	4.0	96.0

3.7 Experimental Equipment and Facilities

3.7.1 Homogenizer

Homogenization process ensures uniform dispersion of the nanoclay throughout the liquid resin. Homogenizer system (*Make: IKA T25 ULTRA-TURRAX, Cole-Parmer, Chicago, US*), as shown in Fig. 3.1, is available at *Chemical Engineering Department, Thapar University, Patiala* is a high performance dispersing instrument for volumes from 1–2000 ml (H_2O) with digital speed display. It offers a wide speed range from 3000–25000 rpm that enables users to work at high circumferential speeds even with small rotor diameters.

Figure: 3.1 Homogenizer
(Photo courtesy: Chemical Engineering Department, Thapar University, Patiala)

Its other advantages include electronic speed control, electronic overload protection, and stainless steel dispersing elements that can be changed quickly and easily, error code display and quiet operation. It is ideal for manual operation, is lightweight with ergonomic form and is equipped with a quick release coupling that simplifies changing and cleaning of the disperser. The dispersion is based on the rotor-stator principle. The rotor is moved with a high circumferential speed. The rotation produces suction, which pulls the medium into the rotor and then pushes it to the outside with help from the stator's teeth. This process results in sample's dispersion. It leads to intensive momentary crushing of liquid droplets and solid particles of preferably small sizes [Web Reference: http://www.ika.com/Dispersing_appl-5.html].

3.7.2 Probe Sonicator

Probe sonication is highly effective for processing nano-materials (carbon nanotubes, nanoclays, graphene, inks, metal oxides, etc.). The ultrasonic electronic generator transforms AC line power to a 20 KHz signal that drives a piezoelectric convertor/transducer.

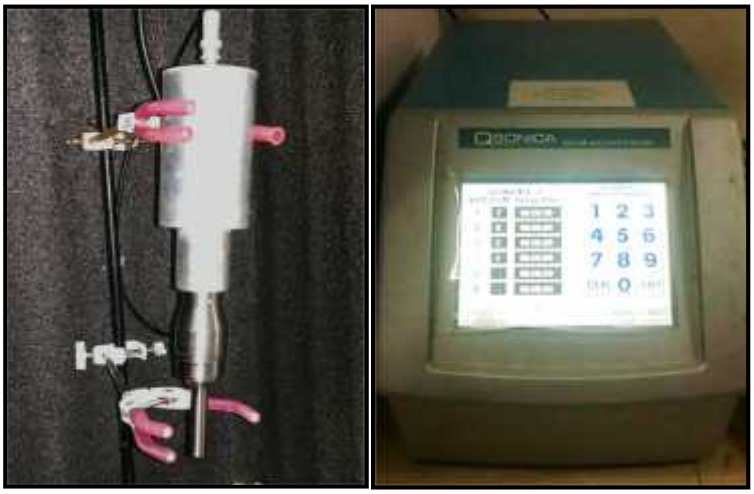

Figure: 3.2 Probe Sonicator
(Photo courtesy: Chemical Engineering Department, Thapar University, Patiala)

This electrical signal is converted by the transducer to a mechanical vibration due to the characteristics of internal piezoelectric crystals. Amplitude (intensity) is controlled from 1–100 % giving a greater degree of resolution and ability to pinpoint the amplitude needed to effectively process the sample. The vibration is amplified and transmitted down the length of the horn/probe where the tip longitudinally expands and contracts. The distance the tip travels is dependent on the amplitude selected by the user through the amplitude control knob. In liquid, the rapid vibration of the tip causes cavitation, the formation and violent collapse of

microscopic bubbles. The collapse of thousand of cavitation bubbles, releases tremendous energy in the cavitation field. Objects and surfaces within the cavitation field are “processed” (Web Reference: http://www.sonicator.com/literature/how-it-works.shtml). Probe Sonicator, as shown in Fig. 3.2 (*Make: Q Sonica Sonicators, Newtown, US*), is available at *Chemical Engineering Department, Thapar University, Patiala*.

3.7.3 Mechanical Stirrer

Once the addition of clay is done in the epoxy, the next step would be to finally add hardener into the clay-epoxy system. This operation is performed during continuous stirring using a mechanical stirrer. The mechanical stirrer has a PMDC motor for powerful stirring alongwith stepless electronic speed regulator with digital display. The stirring shaft and retort rods are made of SS 316 and SS 304 respectively. Its other salient features include reliable performance even in continuous use and, an adaptable chuck for easy interchangeability of shaft [Web Reference: http://www.remilabworld.com/Direct_Drive_Stirrers.asp]. This mechanical stirrer (*Make: REMI Laboratory Instruments, Mumbai, India*), as shown in Fig. 3.3, is available at *Chemical Engineering Department, Thapar University, Patiala*.

Figure: 3.3 Mechanical Stirrer
(Photo courtesy: Chemical Engineering Department, Thapar University, Patiala)

3.7.4 Vacuum Oven

The vacuum oven (*Make: MSW-218, Macro Scientific Works Pvt. Ltd., New Delhi, India*) is suitable for vacuum drying, curing, out-gassing solids and liquids, and, vacuum embedding. It has a microprocessor controlled system implementing superior temperature accuracy along

with superior uniformity and stability. Other features include very easy and convenient vacuuming and venting ports; easy to read vacuum gauge; high quality door sealing made of silicon; highly safe viewing window made of tempered safety glass or thick polycarbonate; over temperature protection; heat transfer from concealed heaters for temperature uniformity and, easy to use. Its internal chamber and sliding shelf is made up of stainless steel (SS 304) and its exterior construction is of steel with heat cured epoxy powder coating [Web Reference: http://www.macroscientificworks.com/ovens-incubators8.html#ove8]. This set-up, as shown in Fig. 3.4, is available at *Chemical Engineering Department, Thapar University, Patiala*.

Figure 3.4: Vacuum Oven
(Photo courtesy: Chemical Engineering Department, Thapar University, Patiala)

3.7.5 Weighing Balance

The analytical weighing balance (*Make: CAS, Korea; Model: CAUW220D*), as shown in Fig. 3.5, is used for weighing clay. Available in *Chemical Engineering Department, Thapar University, Patiala*, this laboratory balance has maximum weight limits of 220 g and measurement resolution of 0.0001 g. Its case material is made of plastic whereas the platform material is stainless steel [Web reference: http://ipelican.com/en/131570].

Figure 3.5: Weighing Balance
(Photo courtesy: Chemical Engineering Department, Thapar University, Patiala)

3.7.6 Universal Testing Machine

The universal testing machine (*Make: Zwick/Roell, Ulm, Germany*) is used to carry out the tensile tests over the samples of the fabricated nanocomposites. It has a capacity of 10 kN, provided with different fixtures for tensile and flexural testing. The UTM can be (*Model: Z010TN, ProLine*) operated at extremely low minimum speeds combined with excellent speed-constancy. The drive also delivers high crosshead travel resolutions which are important in tests on components requiring a high degree of travel-precision and in tests on specimens with high levels of stiffness and low travel, for example [Web Reference: http://senselektro.hu/wp-content/uploads/zwick/ProLine.pdf].

Figure 3.6: Universal Testing Machine
(Photo courtesy: Chemical Engineering Department, Thapar University, Patiala)

The tensile testing samples are prepared according to ASTM D638–02a, which is a standard test method for determination of tensile properties of reinforced and unreinforced plastics in the shape of standard dumbbell-shaped test specimens. This machine, as shown in Fig. 3.6, is available at *Chemical Engineering Department, Thapar University, Patiala*.

3.7.7 X-Ray Diffractometer (XRD)

The X-ray diffraction is used to determine the degree of exfoliation/intercalation of nanoclay between the polymer layers. This technique is based upon Bragg's diffraction law, which is given by the Eq. (3.1):

$$n\lambda = 2d\sin\theta \tag{3.1}$$

whereas, n is an integer, the variable d is the distance between atomic layers in a crystal, the variable λ is the wavelength of the incident X-ray beam and, θ is the certain angle of incidence. The presence of a peak in the XRD curve shows that upto certain degree, intercalation/exfoliation has taken place but not completely whereas, and absence of any peak represents a complete intercalation/exfoliation. This X-ray Diffractometer (*Make: PANalytical, Almelo, Netherlands*), as shown in Fig. 3.7, is available at *SAI Labs, Thapar Technology Campus, Patiala*.

Figure 3.7: X-Ray Diffractometer
(Photo courtesy: SAI Labs, Thapar Technology Campus, Patiala)

The equipment (*Model: X'Pert*^{3} *Powder*) has full ceramic X-ray tubes and a 3 kW generator supporting all current and future X-ray tubes. It has direct optical encoding positioning system (DOPS) for lifetime goniometer accuracy and its maximum usable range (depending on accessories) is $-40^o < 2\theta < 220^o$. A complete data acquisition and analysis software suite

is user-friendly and generates good-quality results right from the start [Web Reference: http://www.panalytical.com/XPert3-Powder/Specifications.htm].

3.7.8 Scanning Electron Microscopy (SEM)

The scanning electron microscopy (SEM) is used for observation of specimen surfaces. When the specimen is irradiated with a fine electron beam (called an electron probe), secondary electrons are emitted from the specimen surface. Topography of the surface can be observed by the two-dimensional scanning of the electron probe over the surface and acquisition of an image from the detected secondary electrons. In the present work SEM (*Make: JEOL Ltd, JSM-6510LV, Tokyo, Japan*), as shown in Fig. 3.8, available at *SAI Labs, Thapar Technology Campus, Patiala* has been used. The low vacuum model provides the versatility of dealing with samples that are wet, oily, outgassed excessively or are non-conductive without pretreatment. It has an accelerating voltage raging 500 V to 30 kV and magnification in the range ×5–300000 [Web Reference: http://www.jeol.com].

Figure 3.8: Scanning Electron Microscope
(Photo courtesy: SAI Labs, Thapar Technology Campus, Patiala)

3.7.9 Vickers Microhardness Tester

Microhardness test is defined as a hardness test using a calibrated machine to force a diamond indenter of specific geometry into the surface of a material being evaluated, in which the test forces are 9.807×10^{-3} to 9.807 N (1 to 1000 gf) and the indentation diagonal,

or diagonals are measured with a light microscope after load removal; for any test, it is assumed that the indentation does not undergo elastic recovery after the force removal. The test results are normally in Knoop or Vickers scale. Vickers hardness number (HV) is an expression of hardness obtained by dividing the force applied to a Vickers indenter by the surface area of the permanent indentation made by the indenter. Microhardness indentation tests extend testing to materials that are too thin or too small for macro-indentation hardness tests. Microhardness indentation tests also allow specific phases or constituents and regions or gradients too small for macro-indentation hardness testing to be evaluated. The Vickers indenter is a square-based pyramidal-shaped diamond indenter with the face angles of 136^{o}. For the micro-range, Vickers hardness test loads are typically in grams-force (gf) and indentation diagonals are in micrometers (µm). The Vickers hardness number is calculated from Eq. (3.2) as follows:

$$HV = 1854.4 \times P/d^2 \tag{3.2}$$

where '*P*' is the force (gf) and '*d*' is the mean diagonal length of the indentation (µm). The ASTM standard followed is E384–$10^{\varepsilon 2}$, which is a standard test method for Knoop and Vickers hardness of materials. This microhardness tester (*Make: Metatech Industries, Model: MHV-1*), as shown in Fig. 3.9, is available at *Advanced Metrology Lab, Mechanical Engineering Department, Thapar University, Patiala*. It has a load range 10–1000 gf, loading/unloading is automatic, dwell time 5–60 s and magnifications available are ×100 and ×400 [Web Reference: http://www.metatechind.com/html/micro.htm].

Figure 3.9: Vickers Microhardness Tester
(Photo courtesy: Mechanical Engineering Department, Thapar University, Patiala)

3.7.10 Low Capacity Izod Impact Tester

For the Izod impact testing, the specimen is in the shape of a bar of square cross section, into which a V-notch is maintained. The load is applied as an impact blow from a weighted pendulum hammer that is released from a cocked position at a fixed height *h*. Upon release, a knife edge mounted on the pendulum strikes and fractures the specimen at the notch, which acts as the point of stress concentration for this high-velocity impact blow. The pendulum continues its swing, rising to a maximum height *h'*. The energy absorption, computed from the difference *h* and *h'*, is a measure of the impact energy [Callister, 2007]. The specimens for izod impact testing is prepared according to ASTM D 256–02$^{\varepsilon 1}$, which is a standard test method for determining the Izod pendulum impact resistance of plastics. The Izod impact tester used in current study (*Make: ATS Faar*), as shown in Fig. 3.10, has the load capacity of 2–25 J and can measure minimum breaking energy 0.001 J. This equipment is available at *Central Institute of Plastics Engineering & Technology (CIPET), Amritsar*. The unit of impact strength shown on display is in Joule (J), which is converted into kJ/m^2 by using the following formulation:

$$Z_{iR} = (W \times 10^3) \div (a \times b_N) \tag{3.3}$$

whereas, Z_{iR} is the impact strength (kJ/m^2), W is the energy absorbed (J) during breaking the test specimen, a is the thickness of the test specimen (mm), and b_N is the remaining width at the notch base of the test specimen (mm).

Figure 3.10: Low capacity Izod Impact Tester
(Photo Courtesy: CIPET, Amritsar)

3.8 Experimental Procedure

This section covers the experimental procedure followed for the fabrication of pure epoxy sample as well as the nanocomposites.

3.8.1 Procedure of Composite Fabrication

1. The first step towards fabrication of composite was to decide the number of samples required for performing each of the mechanical tests (tensile, impact and microhardness testing), under one specific condition. On the basis of this decision, the mold size was selected. In this study, five sample each of tensile and impact tests, and one for microhardness testing were selected for a given composition. For this, the aluminium mold size was selected as 27 × 20 × 1.5 cm^3 to fabricate a master sample. From this master sample, samples for tensile, impact and microhardness testing were cut as per ASTM standard requirements.

2. The next step was to determine the density of resin system to calculate the mass of resin to be poured in the aluminium mold. This required information regarding the density of epoxy and hardener respectively. As specified by the manufacturer, the density of epoxy is 1.15 g/cm^3 and that of hardener is 0.99 g/cm^3. The mass mixing ratio of epoxy and hardener to form the resin system has been defined as 100:35 by the supplier. The volume mixing ratio has been calculated as follows:

   Volume of epoxy = (mass of epoxy) ÷ (density of epoxy) …….(a)

   - Volume of epoxy = (100 ÷ 1.15) = 86.95 cm^3 ……...(a’)

   Similarily,

   Volume of hardener = (mass of hardener) ÷ (density of hardener) …….(b)

   - Volume of hardener = (35 ÷ 0.99) = 35.35 cm^3 ……(b’)

   Thus, a mixing ratio of epoxy and hardener of 100:35 by mass is equivalent to a mixing ratio of 86.95:35.35, by volume.

   Mass of the resin system = mass of (epoxy + hardener) ……..(c)

   - (Volume of resin system) × (density of resin system) = (100 + 35) ……..(c’)
   - $(86.95 + 35.35) \times \rho_r = 135$
   - $\rho_r = 1.1038\ g/cm^3$ ……..(d)

Therefore, density of the resin (epoxy-hardener) system was determined to be 1.1038 g/cm^3.

3. The next step was to determine the mass of resin system to be poured in the mould to fabricate the samples for mechanical testing. For both tensile and impact testing, thickness of samples was taken as 3.2 mm in accordance with ASTM standards. Thus, thickness of master sample was taken as 3.2 mm. thus, the height upto which resin was to be poured in the mould was 3.2 mm. the mass of resin system was determined as follows:

   Mass of resin required in the mould $= \rho_r \times$ volume of the master sample to be fabricated

   ……..……..……..……(e)

- Mass of resin required in the mould $= \rho_r \times$ (area of the mould $\times$ thickness of the samples)
- $m_r = (1.1038) \times (27 \times 20 \times 0.32) = 190.73$ g

4. The next step was to determine the weight of epoxy and hardener separately for the pristine sample. Since, in the resin system, epoxy-hardener is present in weight ratio of 100:35, the individual amount of epoxy and hardener were obtained as follows:

- Amount of hardener required for pristine sample $= (35 \div 135) \times 190.73 = 49.44$ g …..(f)
- Amount of epoxy required for pristine sample $= (190.73 - 49.44) = 141.29$ g …..……(g)

5. The next step was to place an aluminium mold over a levelled surface and justify the levelling using a spirit level. Some packing is required (sometimes) to ensure approximately perfect level conditions.

6. The next step was to make sure that the mold was properly coated with a layer of mold cleaner and a mold releasing agent (*Suppliers: Frekote, Mexico City, Mexico*). In the absence of this coating, the release of the composite from the mold becomes an uphill task, even leading to breaking of the composite or its disfiguring during removal owing to brittle nature of epoxy.

7. Next was to add the hardener into the epoxy with a continuous mechanical stirring at 500 rpm for 7 min for pristine epoxy-hardener system; no clay loading. For this, 141.29 g of epoxy and 49.44 g of hardener had been weighed and kept in separate beakers. The stirrer must be dipped completely in the epoxy and then only the stirring sequence should begin. Even during the stirring, before and after the addition of hardener, the stirrer must be completely dipped into the epoxy/resin system and any sort of up-down motion of the stirrer must be avoided. All these precautions have been listed to ensure that any

entrapment of air must be avoided, as it can lead to pre-mature failure of the sample during testing.

8. Next, the epoxy-hardener resin system was placed in a vacuum oven maintained at a low pressure of 700 mm of Hg. A maximum degassing period of upto 5 minutes was provided (However, this step is optional and if for a given case, curing time is too less, the step can be eliminated).

9. In the next step, resin was poured into the master mould respectively. The spatula was used to remove any visible air bubbles over the surface of the poured resin system before the curing began. The resin system was allowed to cure for 24 h at room temperature and was then removed from the aluminium mold.

10. The above mentioned procedure is for the pure epoxy-hardener system. For fabricating the nanocomposite, having a certain level of clay content, for example say 1.5 wt. % nanoclay content, some new steps had to be included. The calculations regarding weight of clay required to be added in the epoxy are as follows:

    Say, 1.5 wt. % clay must be added into the epoxy.

    The weight of pristine epoxy system = 190.73 g

    Weight of the clay required to be added = (1.5 ÷ 100) × 190.73 = 2.86 g of nanoclay

    Weight of epoxy-hardener required in the nanocomposite system = (190.73 – 2.86) = 187.87 g

    Amount of hardener required in the nanocomposite system = (35 ÷ 135) × 187.87 = 48.70 g

    So, the weight of epoxy required in this nanocomposite = (187.87 – 48.70) = 139.17 g

Table 3.2: Weight percentage of constituents

Sample No.	Clay loading (wt. %)	Amount (in grams) of		
		Clay	Epoxy-hardener	
			Epoxy	Hardener
1	0.0	0.00	141.29	49.44
2	0.5	0.95	140.58	49.20
3	1.0	1.90	139.88	48.95

4	1.5	2.86	139.17	48.70
5	2.0	3.81	138.46	48.46
6	3.0	5.72	137.05	47.96
7	4.0	7.62	135.64	47.47

11. This step describes the preparation steps for the nanocomposites. Firstly, the clay-epoxy mix was homogenized using a homogenizer at 20,000 rpm for 10 minutes. It was made sure that after every 2 minutes cycle of homogenization, the rpm was brought to zero so as to avoid overheating of the system.

12. After homogenization, the final step was sonication of the clay-epoxy mix using a probe sonicator at 80 % amplitude control for 15 minutes. The pulse on time was selected as 30 s whereas the pulse off time is 10 s. During the probe sonication, an ice bath was placed below the beaker because temperature of the system reaches approximately 80 ℃. After this, the hardener was added to epoxy-clay mixture and the same steps as explained in steps 5–9 were followed.

3.8.2 Sample Preparation

The samples for the tensile, and impact testing were cut from the master sample using a circular saw, available at *Central Workshop, Thapar University, Patiala*. The main steps involved are as follows:

1. XRD characterization of all formulations was performed in order to determine the extent of clay intercalation or exfoliation, which is determined the presence or absence of peak in XRD diffractogram. The incidence angle '2θ' is varied in the range 2–10^{o} [Liu *et al.*, 2004; Mohan *et al.*, 2006; Abacha *et al.*, 2007; Gupta *et al.*, 2007; Lim and Chow, 2011; Olad *et al.*, 2012; Kusmono *et al.*, 2013; Al-Qadhi *et al.*, 2013; Al-Qadhi *et al.*, 2014; Sharmila *et al.*, 2014].The powdered samples for XRD were prepared using mixer-grinder.

2. The tensile testing samples were prepared ac1cording to ASTM D638–02a standard. Under this test standard, the Type 1 dimension is selected, which has the following specifications: overall length (*LO*) is 165 mm, overall width (*WO*) is 19 mm, gauge length (*G*) is 50 mm, distance between the grips (*D*) is 115 mm, width of narrow section (*W*) is

13 mm, length of narrow section (*L*) is 57 mm, radius of the fillet (*R*) is 76 mm and finally, the thickness (*T*) of the specimen maintained is 3.2 mm. The speed of testing selected was 5 mm/min. The desired dog bone shape was obtained by grinding the flat pieces manually over a bench grinder. Figure 3.12 shows the tensile test samples.

Figure 3.11: Powder Sample for XRD

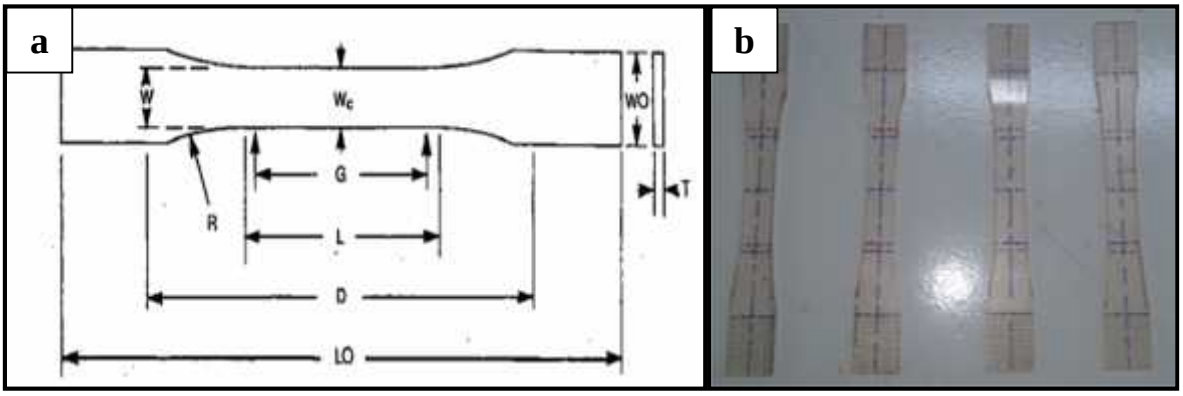

Figure 3.12: Tensile testing samples (a) as per ASTM standard (b) actual sample prepared for experimental work

3. For the izod impact testing, the standard used was the ASTM D 256–02$^{\varepsilon 1}$, which is a standard test method for determining the izod impact resistance of plastics. According to the standard, the specimen dimensions selected were 63.5 × 12.70 × 3.2 mm^3, with a notch angle of 22.5^o and the thickness (denoted as width in figure 3.13) for the molded specimens could be varied between 3.0–12.7 mm. In the present work, thickness of 3.2 mm was selected. The values for *A*, *B*, *C*, *D*, and *E* are 10.16 mm, 31.8 mm, 63.5 mm, 0.25R and 12.70 mm respectively. Figure 3.13 shows the impact test samples.

4. For hardness testing, there is no standard shape or size for a Knoop or Vickers test specimens. To obtain usable information from the test, the specimens have to be prepared or mounted so that the test surface is perpendicular to the axis of the indenter. The thickness of the specimen tested has to be such that no bulge or other marking showing

the effect of the test force appear on the side of the piece opposite the indentation. The specimen size maintained in the present work was 20 × 20 × 3.2 mm^3. A total of twenty indentations were measured on the sample surface as per ASTM E384–$1^{0\varepsilon 2}$, which is a standard test method for Knoop and Vickers hardness of materials. To increase the accuracy of measurement, all sample surfaces were polished using high-grade sand paper (grit size 1000, 1500 and 2000) prior to the test [Rashmi *et al.*, 2011].

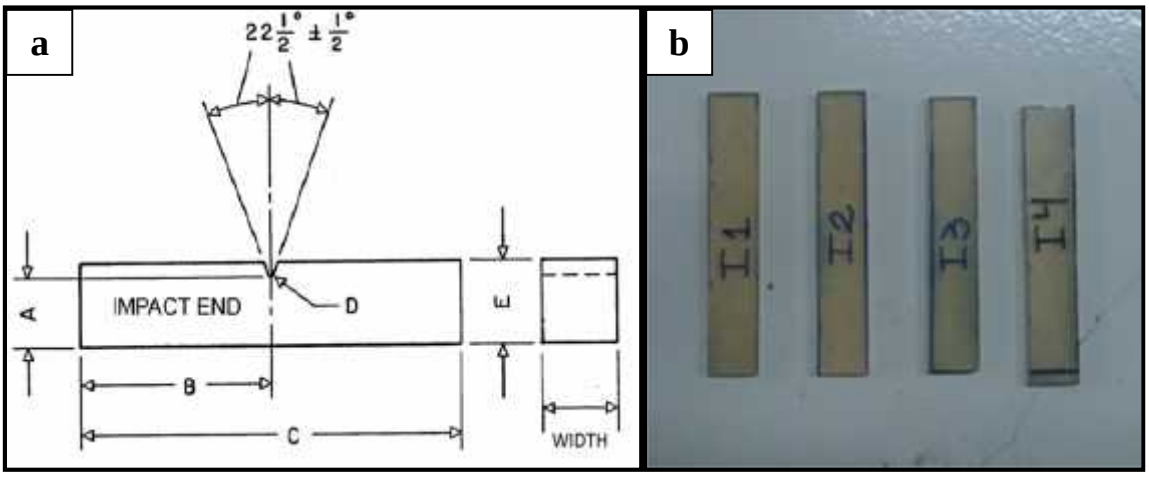

Figure 3.13: Impact testing specimens (a) as per ASTM standard (b) actual sample prepared for experimental work (without notch)

5. In order to carry out SEM, the fractured and worn surfaces of specimens after tensile tests were coated with a few nanometer thick gold sputtering for improving their conductivity [Yasmin *et al.*, 2003; Liu *et al.*, 2004; Dasari *et al.*, 2005; Teh *et al.*, 2005; Wang *et al.*, 2005; Lim and Chow, 2011; Mouloud *et al.*, 2012; Kusmono *et al.*, 2013; Bashar *et al.*, 2014; Sharmila *et al.*, 2014; Kumar *et al.*, 2015].

3.9 Summary of the Chapter

This chapter throws light over the experimental design of the thesis work. It begins with the most important section of this complete study i.e. determination of the objective function and the research methodology followed. After that, the general information regarding input constituents (nanoclay and epoxy) required for the fabrication of nanocomposites has been presented along with their maximum and minimum limits (obtained from the literature). Also, particular nanoclay loading values have been selected in order to study the trend followed by mechanical properties with increasing nanofiller content. In the next section, various equipment, instruments and facilities have been explained which played a major role in the fabrication and testing of the unreinforced and reinforced plastic samples. Finally, the steps

followed and calculations performed for the fabrication of a pristine epoxy and nanoclay reinforced epoxy samples has been discussed alongwith the sample preparation procedures.

Chapter 4
Results and Discussion

4.1 Introduction

This chapter discusses the results obtained with regards to various characterization techniques and mechanical testing performed in the present experimental work. The chapter deals with the results obtained from studying the structure of epoxy-clay nanocomposites and also their fracture surfaces using XRD and SEM characterization techniques respectively. This is followed by reporting and discussing the trends observed in mechanical (tensile, impact and microhardness testing) properties with change in clay loading.

4.2 X-Ray Diffraction (XRD) Analysis

XRD studies were carried out on the pristine nanoclay (Cloisite® 93A MMT), pure polymer and various epoxy-clay nanocomposites (0, 0.5, 1.0, 1.5, 2, 3 and 4 wt. % nanoclay loading) respectively. The patterns obtained are shown in Fig. 4.1.

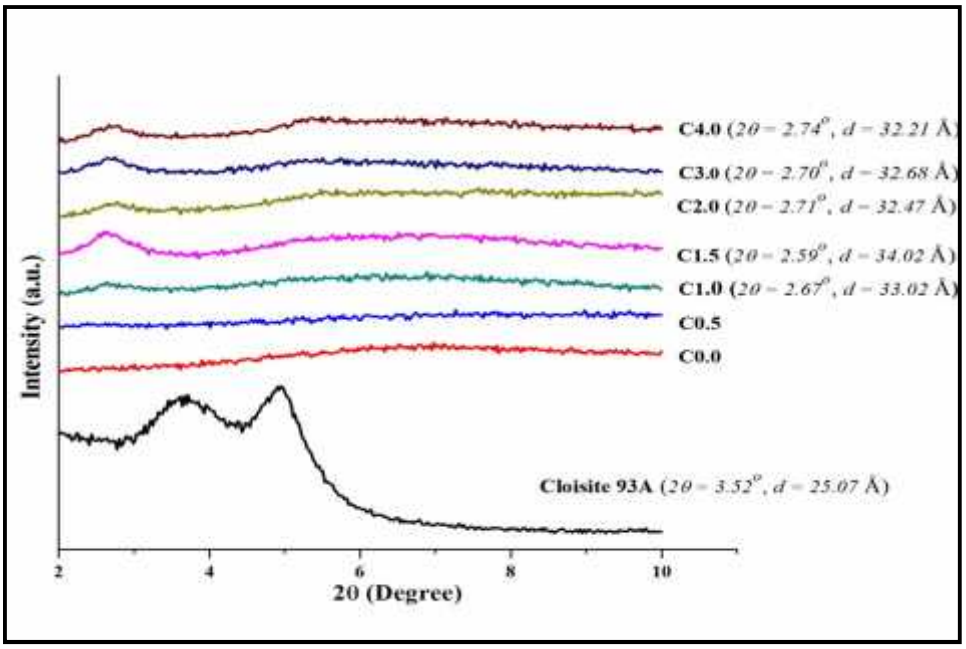

Figure 4.1: XRD patterns of the neat polymer, MMT and nanocomposites

The basal spacing of the pristine nanoclay (Cloisite® 93A) was 25.07 Å corresponding to a broad d_{001} diffraction peak at around $2\theta = 3.52^{o}$. It was observed that the (001) peak of clay in various epoxy/93A nanocomposites shifted to a lower angle as compared to pristine Cloisite®

93A (Table 4.1). The d-spacing increased from the original value of 25 Å (pristine clay) to around 32 Å (nanocomposite with 4 wt. % clay content). The d-spacing was observed to be almost constant in nanocomposites with different amount of nanoclay. However, there was a slight increase in the basal spacing of 1.5 wt. % nanocomposite.

Table 4.1: XRD results of various formulations

Composition (and its designation)	2θ (°)	d-spacing (Å)
Pristine Cloisite® 93A	3.52	25.07
Nanocomposite with 0.5 wt. % clay (C0.5)	**Complete Exfoliation**	
Nanocomposite with 1.0 wt. % clay (C1.0)	2.67	33.02
Nanocomposite with 1.5 wt. % clay (C1.5)	2.59	34.02
Nanocomposite with 2.0 wt. % clay (C2.0)	2.71	32.47
Nanocomposite with 3.0 wt. % clay (C3.0)	2.70	32.68
Nanocomposite with 4.0 wt. % clay (C4.0)	2.74	32.21

The increase in d-spacing represent compatibility of epoxy resin with the layered silicates (nano clay) due to which epoxy chains penetrate into the clay galleries and expand the nano size to some extent [Chozan *et al.*, 2008]. The epoxy nanocomposite with 0.5 wt. % clay loading did not show, however, any peak of a diffraction corresponding to (001) plane after curing; this is attributed in general to two possible reasons: (a) exfoliated structure, or (b) disordered intercalated structure [Mouloud *et al.*, 2012; Kusmono *et al.*, 2013]. The extra-gallery viscous forces and the electrostatic attractive forces that hold the clay stacks together are weakened by the elastic forces offered by the cross-linked epoxy molecules and lead to an increase in basal spacing of the interlayer or gallery. The surface energy is also lowered; thus, epoxy molecules are able to penetrate into the clay galleries. All these contribute to a better dispersion and intimate interaction between the nanoclay and polymer chains and finally lead to exfoliation [Park and Jana, 2003; Lim and Chow, 2011].

The presence and shift of (001) diffraction pattern indicates coexistence of intercalated and exfoliated structure in the nanocomposite system [Wang *et al.*, 2005]. The observation of peak in the nanocomposite diffractograms revealed that the fabricated nanocomposites still contained clay tactoids. This could also be because of the residue silicate layers that got partially delaminated during the mixing process and not fully delaminated [Lim and Chow, 2011]. This observation was an indication that a single or double layer of epoxy polymer chains were intercalated between the clay nanolayers which eventually expanded the basal spacing of clay during the mixing process [Mouloud *et al.*, 2012]. The

absence of exfoliated morphology could be attributed to the increased intercalating sites with increased clay content that might have impeded the exfoliation of individual silicate layers. Therefore, it can be suggested that the 0.5 wt. % clay nanocomposite showed complete exfoliation with respect to shear force and processing time applied in this study, whereas, the addition of higher clay contents (> 0.5 % clay) produced only an intercalated structure. The high viscosity of resin (due to increased amount of nanoclay in it) as well as the strong tendency of nanoclay particles to agglomerate might also have impeded the exfoliation process. The increase in viscosity of resin due to higher clay content does not allow long chains of epoxy to diffuse into the silicate galleries. In general, the degree of exfoliation/intercalation depends on the type of clay and its surface modification, processing time, processing temperature, nature of curing agent, and the mixing conditions [Yasmin *et al.*, 2003; Mohan *et al.*, 2006; Akbari and Bagheri, 2007]. However, an XRD pattern with an intercalated peak may not always fully reveal relative levels of exfoliation or intercalation. For example, some clay particles do not display well-defined basal reflections and it is difficult to determine the intensity pattern and shape of the relative peaks. These considerations make XRD data only a useful approximation to the nanostructure [Liu *et al.*, 2004].

4.3 Mechanical Properties of Epoxy-Clay Nanocomposites

This section deals with the results of tensile, impact, and microhardness testing of various formulations prepared in the present work.

4.3.1 Effect of Clay Addition on Tensile Properties

A) Effect on Tensile Modulus

Table 4.2 presents the results of tensile modulus obtained for the pure epoxy and different epoxy-clay nanocomposite formulations.

Table 4.2: Mechanical properties of pure epoxy and epoxy-clay nanocomposites

Sample Code	Tensile Strength (MPa)	Tensile Modulus (MPa)	Strain at Break (%)	Impact Strength (kJ/m^2)	Microhardness (Hv)
C0.0	36.30	2576	1.70	1.32	31.79
C0.5	48.96	3950	1.54	1.36	39.10

C1.0	51.95	4055	1.42	1.58	43.27
C1.5	53.72	4074	1.36	1.61	45.81
C2.0	34.40	4108	1.14	1.57	44.85
C3.0	31.82	4200	1.10	1.39	39.89
C4.0	31.78	3664	1.10	1.33	37.97

The tensile modulus of nanocomposites increased for most of the range of clay loadings. It increased upto 3 wt. % nanoclay content, followed by a decreasing trend, as observed in Fig. 4.2 (see Annexure-I). Similar results have been quoted by other authors [Abot *et al.*, 2003; Isik *et al.*, 2003; Yasmin *et al.*, 2003; Basara *et al.*, 2005; Wang *et al.*, 2005; Gupta *et al.*, 2007; Khanbabaei *et al.*, 2007; Chozan *et al.*, 2008; Rashmi *et al.*, 2011; Mouloud *et al.*, 2012; Ngo *et al.*, 2012; Olad *et al.*, 2012; Kusmono *et al.*, 2013].

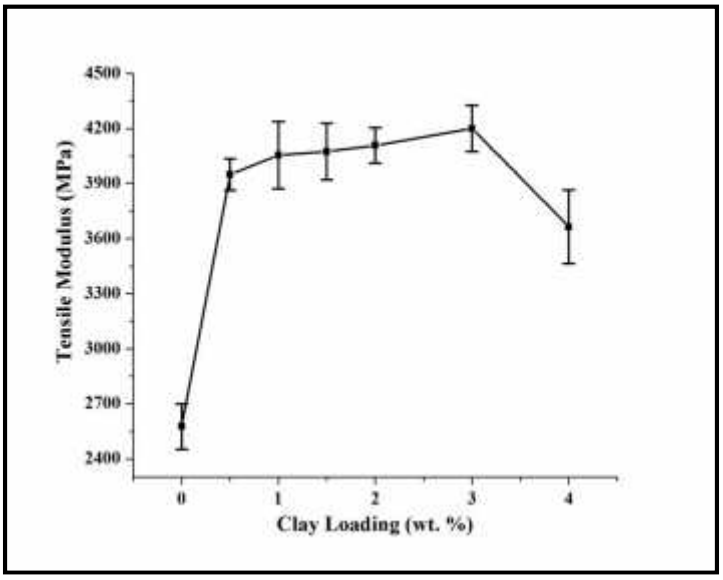

Figure 4.2: Effect of clay addition on tensile modulus

The value of tensile modulus for pure epoxy-hardener system was 2576 MPa which increased to 4200 MPa for 3 wt. % clay content, signifying an improvement of about 63 %. The modulus of a composite depends on the ratio of filler modulus to matrix material modulus. Since, montmorillonite has a higher modulus than the polymeric matrix, the modulus increases with the clay content [Isik *et al.*, 2003]. The added stiffness achieved through the incorporation of nanoclay particles results into achieving an optimum value for the elastic modulus because clay is more rigid than the matrix [Gupta *et al.*, 2007; Khanbabaei *et al.*, 2007]. This response is characteristic for materials reinforced with stiff fillers. The improvement in elastic modulus could also be attributed to the good dispersion of nanoparticles in the epoxy matrix which restricts the mobility of polymer chains under

loading. Improvement can also be because of the good interfacial adhesion between the nanoclay and epoxy matrix. The orientation of clay platelets and polymer chains with respect to the loading direction could also contribute to the reinforcement effect [Yasmin *et al.,* 2003; Mouloud *et al.,* 2011]. The decreasing rate of elastic modulus after 3 wt. % nanoclay content could be attributed to the presence of unexfoliated aggregates in the structure of the resin [Yasmin *et al.,* 2003; Mouloud *et al.,* 2011]. The agglomerated clay particles decrease the polymer-clay surface interactions and also prevent the entering of matrix resin in between the silicate layers [Basara *et al.,* 2005].

B) Effect on Tensile Strength

The tensile strength of the epoxy-clay nanocomposites showed an increasing trend with clay loading upto 1.5 wt. % nanoclay content, followed by a decreasing trend, as observed in Fig. 4.3 (see Annexure-I). The maximum improvement observed in tensile strength was about 48 %, compared to neat epoxy.

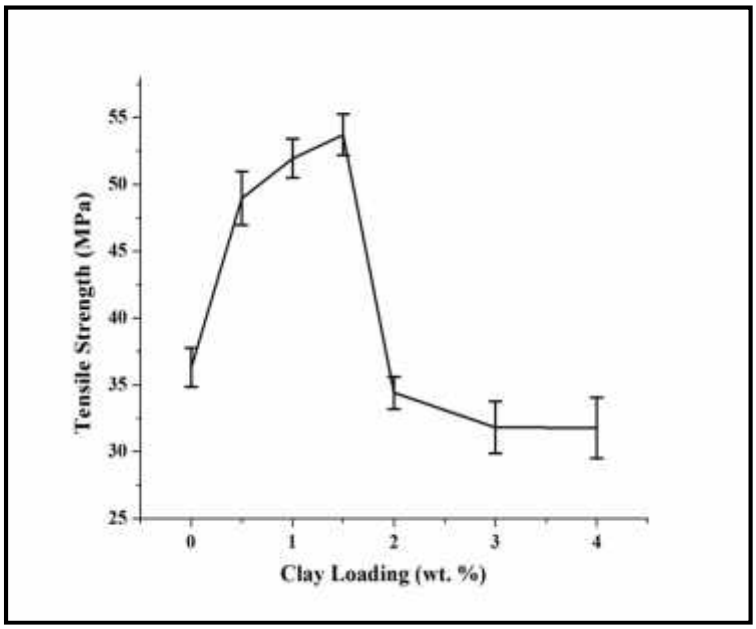

Figure 4.3: Effect of clay addition on tensile strength

Tensile strength of the pure epoxy sample and the composite containing 1.5 wt. % nanoclay was 36.30 MPa and 53.72 MPa respectively. This indicated the reinforcing capability of the intercalated clay particles. Similar trend has been reported in literature by other authors [Basara *et al.,* 2005; Gupta *et al.,* 2007; Chozan *et al.,* 2008; Lingaraju *et al.,* 2011; Ngo *et al.,* 2012; Kusmono *et al.,* 2013]. The high aspect ratio of nanoclay increases the tensile strength by increasing the nanofiller contact surface area on the polymer matrix. Large

number of reinforcing nanoclay platelets present in the polymer matrix act as efficient stress transfer agents in the nanocomposites, inducing plastic deformation into the base polymer, and finally increasing the tensile strength [Kusmono *et al.,* 2013]. However, upon further clay loading, the tensile strength values showed a decreasing trend. Several reasons are possible for this decrease in tensile strength. One is the existence of flaws in the nanocomposites after a particular filler content. These flaws include weak boundaries between nanoclay particles and microsized air bubbles entrapped during the sample preparation. The number of these flaws may increase with the volume fraction of the filler. Another possibility is the inhomogeneous network density of the samples. During the preparation of nanocomposites, the viscosity of epoxy/clay mixture becomes very high due to the dramatically increased interfacial area and the interfacial interaction between the intercalated clay and the epoxy resin. This high viscosity inevitably introduces heterogeneity in the resultant samples. The heterogeneous dispersion of nanoparticles according to increment in resin's viscosity could also be mentioned as an important factor in deteriorating the tensile strength. As the interfacial area of the particles is high, their interaction with epoxy chain would cause lower homogeneity in crosslink density. Moreover, the stress concentration effect of the stacked layer structure of clay minerals due to intercalation phenomenon could also be responsible for decrease in the tensile strength [Wang *et al.,* 2005; Nikje *et al.,* 2009; Olad *et al.,* 2012]. During the mixing of nanoclay and epoxy, a highly viscous and foamy material was formed. Higher the clay content, higher the viscosity of composite system. The Cloisite® 93A nanoclay accelerated the curing process of the epoxy resin. Therefore, the mixture became highly viscous with time and hindered the complete degassing before casting. Moreover (according to the supplier of epoxy), the gel time available with the hardener Aradur® 837 was 23 minutes. This hindered the practice of following long (significantly more than 23 min) degassing periods as suggested in different literatures [Liu *et al.,* 2004; Basara *et al.,* 2005; Lam *et al.,* 2005; Wang *et al.,* 2005; Zunjarrao *et al.,* 2006; Lim and Chow, 2011; Rashmi *et al.,* 2011; Al-Qadhi *et al.,* 2013; Bashar *et al.,* 2014; Kumar *et al.,* 2015]. Hence, it was observed that the degassing problem became critical for nanocomposites with higher clay loadings, which in turn, produced composites with material defects (i.e. voids, holes etc. due to air entrapment). The other sources of voids could be trapped air during pouring of highly viscous material into the mold. The failure of all specimens (containing higher clay loadings, $\geq$ 2 wt. % clay) at almost similar strength level (31–34 MPa) also indicated the possibility of crack initiation from similar type of material defects (i.e. voids, holes etc. due to air

entrapment). Therefore, under tensile loading, cracks initiate from these tiny voids and cause specimen to fail at relatively low strain, as also reported by Yasmin *et al.* (2003).

C) Effect on Strain at Break

The strain at break values decreased continuously with increasing clay content, as shown in Fig. 4.4 (see Annexure-I) . A few authors have reported a similar trend [Khanbabaei *et al.*, 2007; Olad *et al.*, 2012]. The maximum value observed was 1.7 % for the pure epoxy sample and it got reduced to 1.1 % at 4 wt. % clay loading which means about 54 % reduction in strain at break.

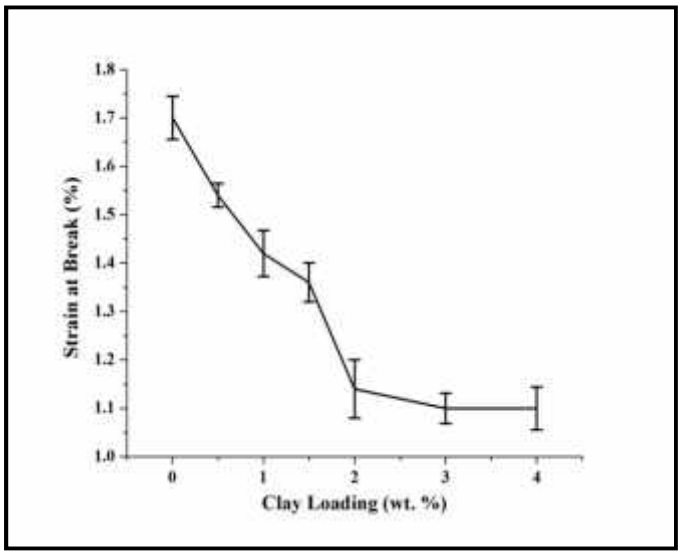

Figure 4.4: Effect of clay addition on strain at break

The reason behind this decreasing trend is that in these composites, the rigid fillers cannot elongate much. The clay particles are rigid fillers and they make the nanocomposite more brittle at high clay contents [Basara *et al.*, 2005; Khanbabaei *et al.*, 2007]. The fillers dominate and reduce the matrix deformation considerably [Mohan *et al.*, 2006].

D) SEM Analysis of Tensile Specimens

SEM micrographs provide important insights regarding clay distribution, particle-crack interaction, and particle-matrix interface, and help in better understanding of the processing-structure-property relationships [Zunjarrao *et al.*, 2006]. From SEM fractograph of the tensile fracture surface of neat epoxy (Fig. 4.5a), two distinct regions were identified (Region A and Region B), each showing a different fracture feature. It was observed that as the load was applied during tensile testing, the cracks initiated at the beginning of region A. These cracks started to advance at a slow rate in region A leaving smooth appearance of fracture surface

(in region A). Once the cracks reached critical size at the end of region A, they propagated at a high rate and resulted in a coarse surface of region B, as reported by Al-Qadhi *et al.* (2013) also.

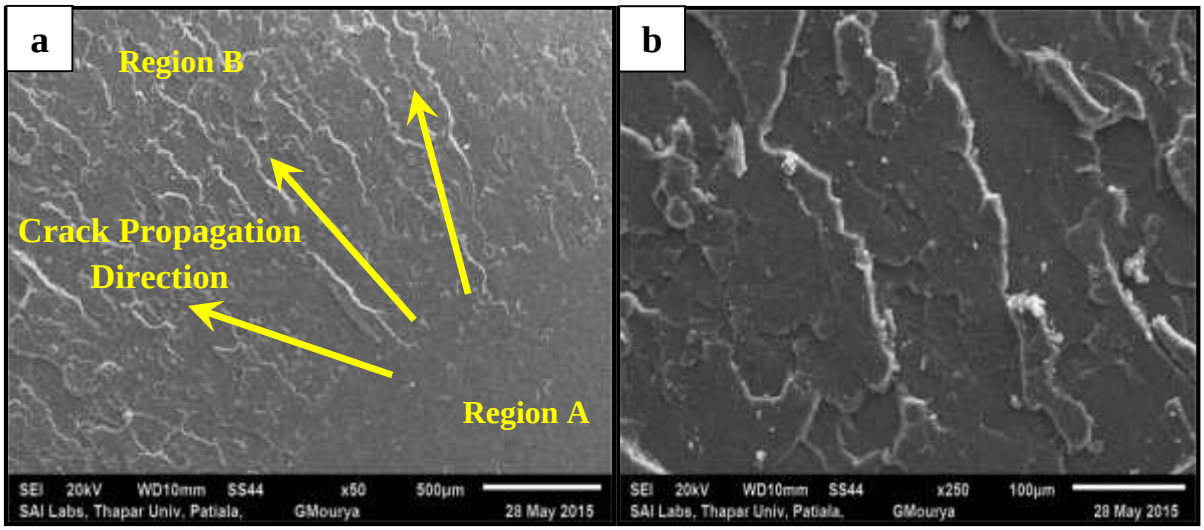

Figure 4.5: SEM micrograph of tensile fracture surface of neat epoxy at: (a) ×50 and (b) ×250

It can be seen in Fig. 4.5b that neat epoxy resin exhibits a relatively smooth surface with occasional river patterns (also crack propagation is largely in one specific direction). This shows that the resistance of material under crack propagation is very less and leads to brittle failure, thus accounting for low tensile strength of cured pure epoxy, as also reported by Sharmila *et al.* (2014). SEM micrograph of the 1.5 wt. % clay nanocomposite shows (see Fig. 4.6a) a fractured surface which is rough (with crack propagation in several different directions; unlike pure epoxy case, where it was largely unidirectional). This morphology indicates that stress in the material was effectively dispersed to various directions. The load energy was considerably dissipated by many factors during crack propagation, and some cracks terminated due to lack of energy, as reported by Li *et al.* (2011) and Olad *et al.* (2012) also. The fractured surface of neat polymer displays a smooth fracture comprising of a river like fracture morphology characterized by long unidirectional cracks without significant presence of mechanisms like crack deflection, crack pinning and/or crack arresting (see Fig. 4.5a–b). On the contrary, polymer nanocomposite (1.5 wt. % clay) displays a much rougher fractured surface characterized by shorter cracks (in various directions) with significant presence of energy absorption mechanisms like crack deflection (a crack travelling in a given straight line deflects from its initial trajectory during the course of its propagation), crack pinning (crack fronts from two different fracture planes meet each other after being after being blocked by inclusions, here nanoclay particles/agglomerates/clusters etc.), and crack

arresting (crack propagation ceases on reaching an inclusion due to lack of sufficient energy) (see Fig. 4.6a–b).

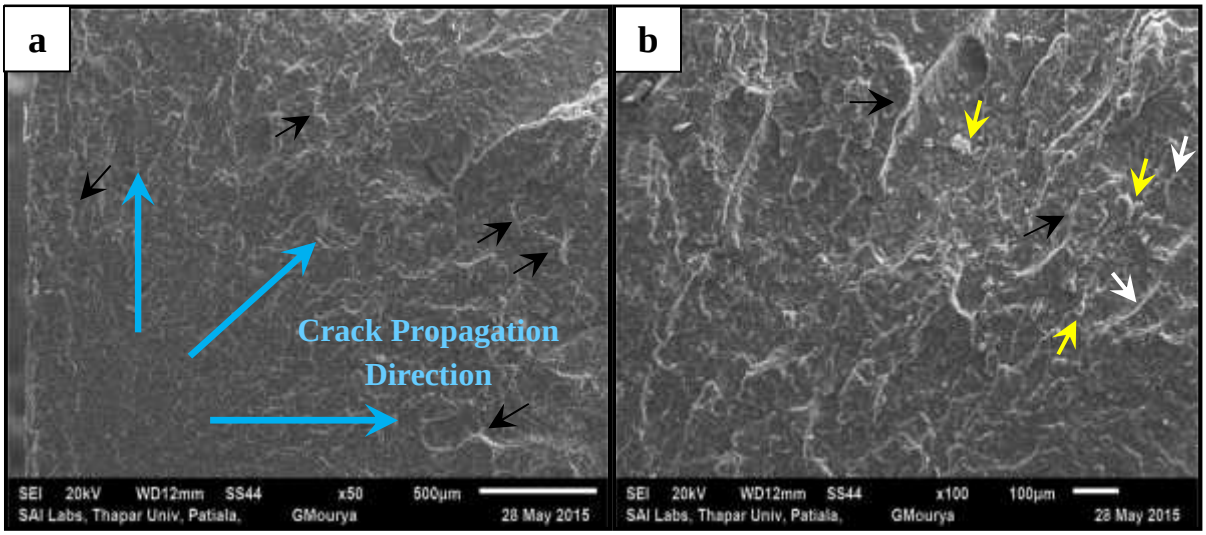

Figure 4.6: SEM micrographs of tensile fracture surface of 1.5 wt. % clay (a) ×50 and (b) ×100

Thus, on addition of nanoclay, the failure surface becomes more rough which makes crack propagation difficult and thereby increases the tensile strength. Hence, crack propagation follows a torturous path for failure in nanocomposites and leads to high strength, as also reported by Sharmila *et al.* (2014). The fracture surface of nanocomposite is a rough corrugated surface displaying a marked departure from the smoother brittle cleavage type fracture for neat epoxy. The roughness of fractured surface in nanocomposite system can be attributed to the change in crack direction as a result of presence of clay in the crack path leading to crack retardation [Al-Qadhi *et al.*, 2011]. The cracks in fractured surface of nanocomposite are fine, close, short, twisting, varying in shape, and scattered in various directions [Li *et al.*, 2011]. At high clay loadings, owing to difference in the scattering density between the clay and epoxy, large aggregates can be easily observed. SEM micrographs of nanocomposite containing 4 wt. % clay showed that as the clay concentration in the nanocomposite increases, large agglomerates of particles are observed and roughness of the fractured surface further increases [Basara *et al.*, 2005; Bashar *et al.*, 2014], as observed in Fig. 4.7a–c. The lowest value of tensile properties (amongst nanocomposite formulations) was observed at 4 wt. % clay loading, may be because agglomerates gave rise to lower clay-polymer surface interactions and higher stress concentrations, as also reported by Basara *et al.* (2005). Moreover, the aggregated Cloisite layers may also have acted as points of stress concentration, which initiated cracks and made them larger than the critical crack size causing early failure, also reported by Sharmila *et al.* (2014).

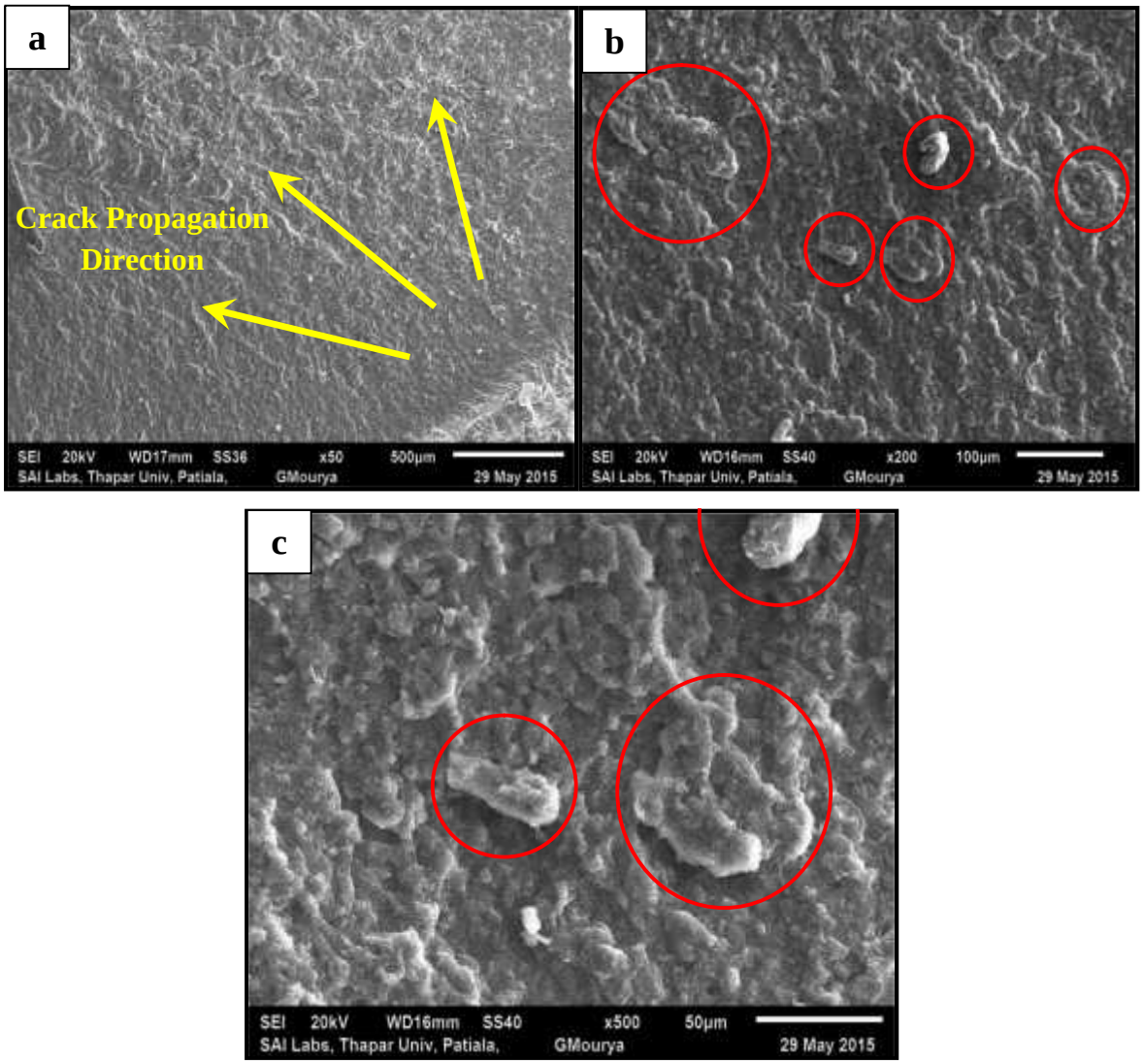

Figure 4.7: SEM micrograph of 4 wt. % clay nanocomposite showing increased roughness at: (a) ×50 (b) ×200 and showing clay agglomerates at: (c) ×500

Also, Yasmin *et al.* (2003) reported that these loose clusters or unexfoliated particles in the matrix may act as additional crack initiation sites by splitting up easily under applied load.

4.3.2 Effect of Clay Addition on Impact Properties

Table 4.2 shows the impact properties of pure epoxy and different epoxy-clay nanocomposite formulations (see Annexure-II). The impact strength of epoxy-clay nanocomposites showed an increasing trend with clay loading upto 1.5 wt. % nanoclay content, followed by a decreasing trend (see Fig. 4.8). The nanocomposite containing 1.5 wt. % nanoclay exhibited the highest value of impact strength (1.61 kJ/m^2), an improvement of about 22 % as compared to unmodified epoxy (1.32 kJ/m^2).

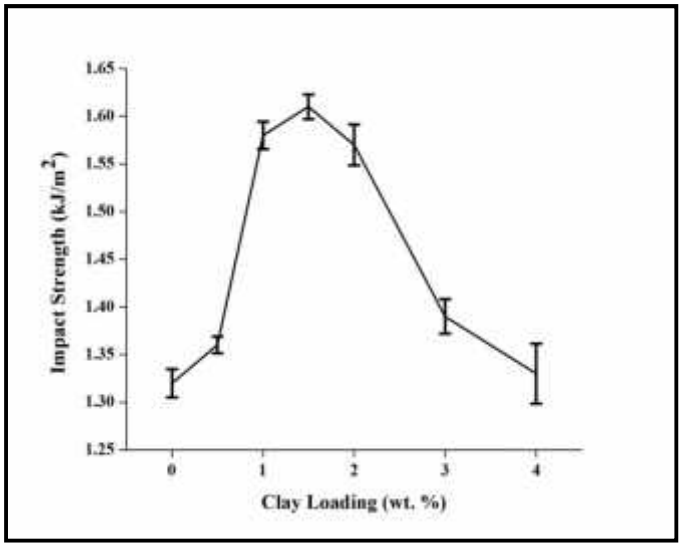

Figure 4.8: Effect of clay addition on impact strength

Similar results have been reported by other authors [Isik *et al.,* 2003; Basara *et al.,* 2005; Mohan *et al.,* 2006; Bakar *et al.,* 2012; Mouloud *et al.,* 2012; Kusmono *et al.,* 2013]. Nanoclay intercalation is considered as the mechanism for improvement in epoxy resin. The clay particles seem to act as crack stoppers and form torturous crack propagation path, resulting in higher impact energy [Basara *et al.,* 2005; Mouloud *et al.,* 2012; Kusmono *et al.,* 2013]. The improvement of impact strength at only low clay contents may be attributed to presence of agglomerates of clay particles at higher clay concentrations, which act as stress concentrators [Isik *et al.,* 2003; Basara *et al.,* 2005; Mohan *et al.,* 2006; Mouloud *et al.,* 2012; Kusmono *et al.,* 2013].

A) SEM Analysis of Impact Specimens

To further understand the structure-property relationship and to possibly explain the toughening mechanism induced by MMT clay, SEM analysis of the fractured surfaces was conducted. Fracture surface of the pure epoxy (see Fig. 4.9) was quite smooth and flat except for some river like markings, which indicates brittle fracture behaviour corresponding to poor impact strength, as also reported by Wang *et al.* (2005) and Mouloud *et al.* (2012). It shows that the resistance of material under crack propagation is less and leads to brittle failure [Mohan *et al.,* 2006]. The crack propagation lines are almost parallel to each other indicating very fast and straight crack propagation [Basara *et al.,* 2005; Kusmono *et al.,* 2013]. The fracture surface of pristine epoxy is smooth glassy surface with a few of sharp and straight paths running through the material along the direction of crack propagation [Lim and Chow, 2011]. Fig. 4.9 shows a smooth and featureless fracture surface of the unfilled epoxy

representing insignificant matrix deformation that is usually observed in a homogeneous brittle material, also reported by Bashar *et al.* (2014). The cracks are in different planes but in almost parallel direction, as indicated by a white arrow also reported by, Liu *et al.* (2004). The cracks, although showing some deflection, stretch mainly in one direction also reported by Li *et al.* (2011).

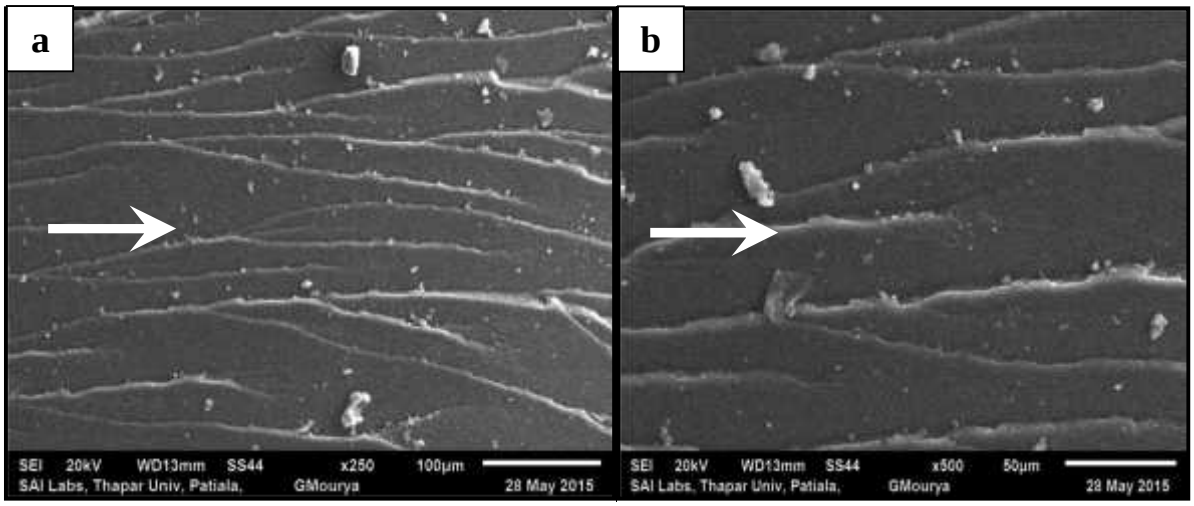

Figure 4.9: SEM micrographs of the fracture surface of neat polymer at: (a) ×250 and (b) ×500

Fracture surface under impact test of 1.5 wt. % nanoclay composite showed increase in roughness and a torturous path indicating difficult crack propagation, leading to high impact strength [Mohan *et al.*, 2006; Mouloud *et al.*, 2012]. Increased surface roughness implied that path of crack tip was distorted because of the clay platelets, making crack propagation more difficult. Even though the clay layers were of the order of 1 nm thickness, it is observed that some of these systems remain in tactoids. A few clay aggregates were observed on the fracture surface and distinct agglomerations are indicated by red circles (see Fig. 4.10). These distinct agglomerates are able to readily interact with the growing crack front. Therefore, the presence of clay particles or agglomerates may cause perturbations along the crack front, thus altering the path of the propagating crack from the straight unperturbed growth seen in the neat resin [Liu *et al.*, 2004]. Wang *et al.* (2005) reported that clay aggregates are exposed on the surface because cracks penetrated through them. As a result, improvement in impact strength can also be attributed to breakage of clay aggregates.

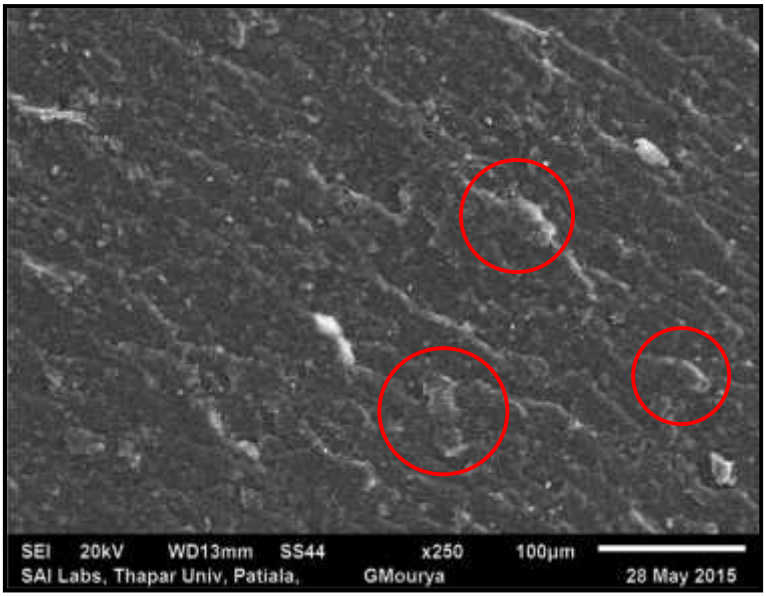

Figure 4.10: SEM micrograph of fracture surface of 1.5 wt. % clay nanocomposite showing distinct clay agglomerates (× 250)

It is known that in a brittle matrix, when a crack front is obstructed and pinned down by a rigid well-bonded particle, the crack becomes bowed out between the particles, resulting in secondary cracks. Consequently more energy would be necessary to propagate this new nonlinear crack front, which also depends upon the particle size and interparticle spacing. It is conjectured that these intercalated clay assemblies are in fact very efficient in inhibiting the crack propagation by pinning mechanism [Bashar *et al.,* 2014]. Crack deflection (indicated by black arrows), crack arresting (indicated by white arrows) and crack pinning (indicated by yellow arrows) are mechanisms favoring improved impact resistance and are indicated in Fig. 4.11. Moreover, an increase in fracture surface roughness is an indicator of crack deflection mechanism, which increases the absorbed energy of fracture by increasing the crack length during deformation [Kusmono *et al.,* 2013]. Other energy absorption mechanisms (apart from crack deflection) include crack pinning and crack arresting, which lead to torturous path followed by crack before failure, responsible for high impact strength [Sharmila *et al.,* 2014]. Characteristic pinning tails can be seen in the SEM image (see Fig. 4.11a–b) which form when crack fronts from two different fracture planes meet each other after being blocked by inclusions.

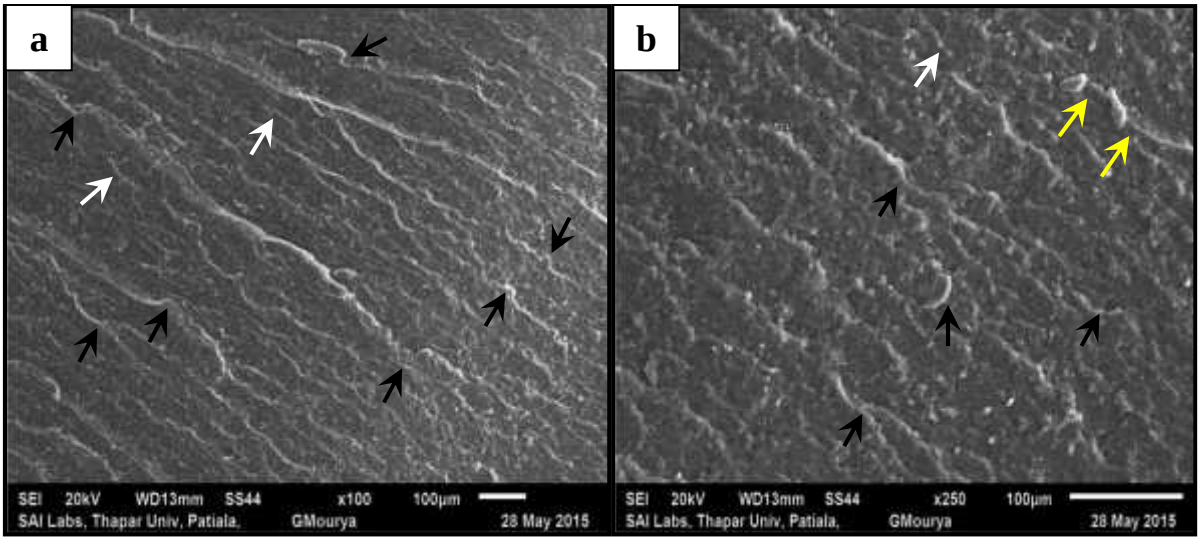

Figure 4.11: SEM micrograph of fracture surface of 1.5 wt. % clay nanocomposites showing crack deflection, crack pinning and crack arresting mechanisms (a) ×100 and (b) ×250

At higher magnifications (×1000 and ×5000), a representative fractographic feature, microvoids, can be clearly observed (indicated by red arrows) in Fig. 4.12.

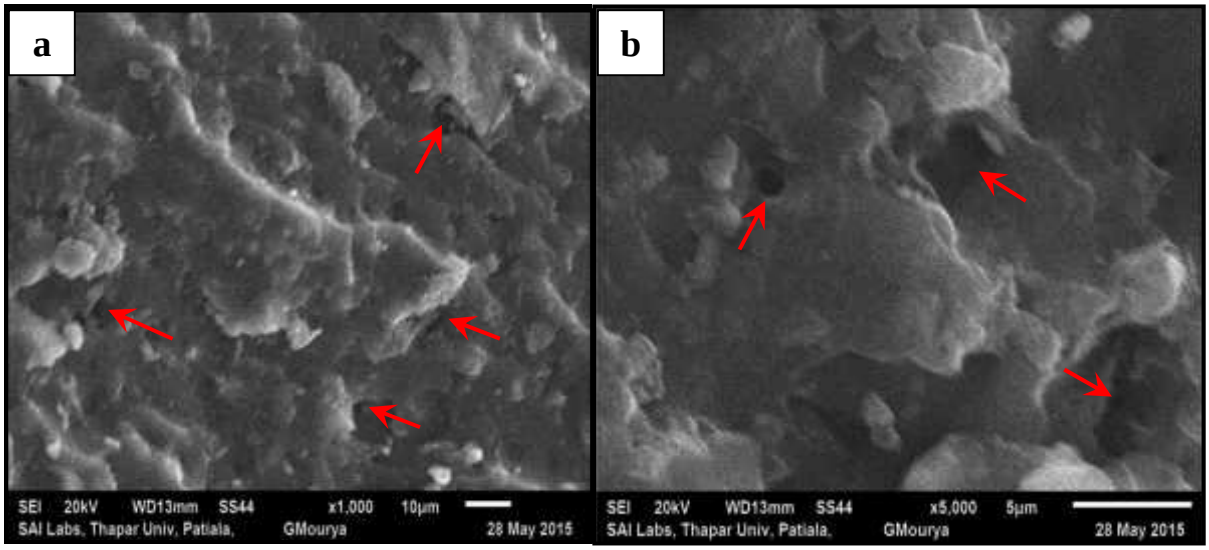

Figure 4.12: SEM micrograph of fracture surface of 1.5 wt. % clay nanocomposites showing microvoids at (a) ×1000 and, (b) ×5000

Upon fracture of the nanocomposite, the clay particles are very likely to be the stress concentration sites because the rigid silicate particles have very different elastic properties as compared to the neat epoxy. This difference in the elastic properties of constituents results in (i) debonding of the clay-matrix interface and (ii) cleavage of clay tactoids, consequently producing some microvoids or nanovoids. These voids could (a) initiate shear yielding of the epoxy matrix at the crack propagation tips and also throughout the entire volume, and/or (b) deform, absorbing more energy before fracturing. Another toughening mechanism called

crack tip blunting can also take place due to localized shear yielding and damage zones such as debonding of the particle-matrix interface and cleavage of clay particles (delamination within silicate layers) [Liu *et al.*, 2004; Lim and Chow, 2011]. The main toughening effect is due to debonding and subsequent plastic deformation of the epoxy polymer around the particles [Mouloud *et al.*, 2012]. These microvoids (also coined as 'macrocracks' by Wang *et al.*, 2005), as shown in Fig. 4.12b, were observed in the interfacial region (interface between clay aggregates/clusters and bulk epoxy matrix) revealing that the physical properties (such as modulus and Poisson's ratio) inside the clusters and outside the clusters (nearby interfacial bulk epoxy matrix) are different. This heterogeneity resulted in stress concentration effect of nanoclay and hence interfacial failure at the epoxy-clay interface [Bashar *et al.*, 2014]. Shear yielding or debonding of the filler-matrix interface will occur when the local stress exceeds the yield stress of neat epoxy or the interfacial strength of the filler-matrix interface [Lim and Chow, 2011]. Although, shear banding has been frequently reported in literatures as one of the major toughening events in epoxy based composites or blends but such a mechanism was not observed in the current epoxy-clay nanocomposite systems. Moreover, as observed in Fig. 4.12a, the resin-clay interface was debonded at a few locations, leading to the generation of few voids. This evidenced a high interfacial force between organoclay-matrix under stress due to the fact that nanocomposite had achieved intercalation. The strong interfacial interactions increased the efficiency of the clay in toughening the resultant nanocomposite by means of effective transfer of stress between the clay and the matrix which accounted for the capability to absorb more energy prior to fracture [Lim and Chow, 2011].

Fig. 4.13 shows the SEM micrograph of fracture surface of 1.5 wt. % clay nanocomposite showing microcracks. The fracture surface was very rough and filled with scalelike steps, indicating that the presence of nanoclay layers forced the cracks to propagate along a very torturous path. Many microcracks were observed located between the scalelike steps, as shown in Fig. 4.13 (indicated by blue arrows), which were perpendicular to the fracture surface. This implied that the action of clay layers as stress concentrators promoted the formation of a large number of microcracks when sample was loaded, as also reported by Wang *et al.* (2005).

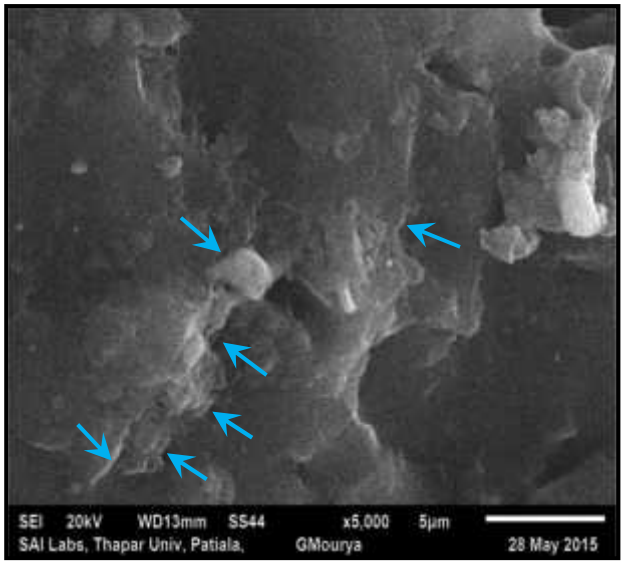

Figure 4.13: SEM micrograph of fracture surface of 1.5 wt. % clay nanocomposites showing microcracks (×1000)

Hence, the enhanced impact strength of the nanocomposite was attributed to the fact that some of the applied energy is dissipated by the debonding of clay-matrix, cleavage or splitting of the clay tactoids. Moreover, the voids were likely to be deformed and absorbing more energy before fracturing and hence again contributed to an increase in impact resistance [Lim and Chow, 2011].

4.3.3 Effect of Clay Addition on Microhardness

Table 4.2 presents the results of microhardness values obtained for the pure epoxy and different epoxy-clay nanocomposite formulations (see Annexure-III). The hardness value represents the ability of a material to stand firm to the local surface deformation. It also indicates the degree of compatibility between clay and epoxy resin as well as degree of cross link density (CLD) among epoxy monomers after polymerization reaction (curing) [Sharmila *et al.,* 2014]. The microhardness showed an increasing trend till 1.5 wt. % nanoclay loading, followed by a decrement in values with increasing clay content. The microhardness value for neat epoxy sample was 31.7 Hv, which got increased to 45.8 Hv, signifying an improvement of about 44.5 %, as shown in Fig. 4.14. Similar trends of hardness have been quoted by other authors [Lam *et al.,* 2006; Chozan *et al.,* 2008; Zaarei *et al.,* 2010; Lingaraju *et al.,* 2011; Rashmi *et al.,* 2011; Olad *et al.,* 2012; Wang *et al.,* 2013; Sharmila *et al.,* 2014]. The higher Hv value of 1.5 wt. % clay nanocomposite could be partly attributed to the intrinsic hardness of MMT and partly to the fact that nanoparticles impose better resistance against epoxy segment motion under indentation [Rashmi *et al.,* 2011].

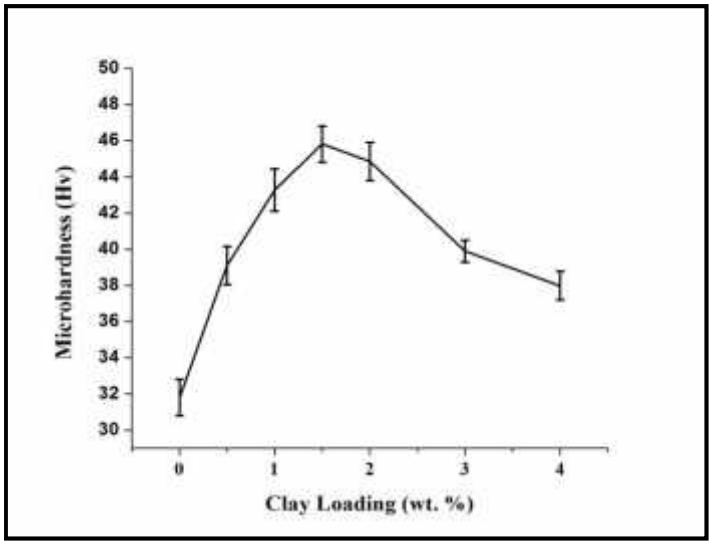

Figure 4.14: Effect of clay addition on microhardness

This enhancement in microhardness could be potentially due to the increased confinement of epoxy resin in 1.5 wt. % clay nanocomposite due to intercalated clay morphology, effectively restricting surface deformation. Moreover, effective dispersion of nanosized clay particles as well as good interfacial adhesion between particles and epoxy matrix could be held responsible for increased hardness [Zaarei *et al.*, 2010; Sharmila *et al.*, 2014]. The decrease in microhardness values at higher clay loadings (> 1.5 wt. %) could be attributed to the fact that the time required for solidification becomes longer for the samples with high nanoclay content as well as the surface of the samples become relatively soft compared to low clay loading nanocomposites. It is suspected that the nanoclays might retard the chemical reaction, and so cause incomplete curing process of the composites. Hence, for all the samples with high nanoclay content, the matrix might not be fully cured [Lam *et al.*, 2005]. Moreover, higher filler loading gives rise to poor dispersion and agglomeration in the epoxy matrix causing a decrease in hardness values [Rashmi *et al.*, 2011; Sharmila *et al.*, 2014].

4.4 Summary of the Chapter

This chapter discussed the results obtained from XRD characterization, mechanical testing (tensile, impact and microhardness testing) of different epoxy-clay formulations, and SEM fractographic images. XRD revealed that 0.5 wt. % nanoclay composite showed complete exfoliation, characterized by absence of peak on diffractogram whereas intercalated structure was obtained for all other nanocomposites. The d-spacing of pristine clay was 25.07 Å, which got increased to 34.02 Å for 1.5 wt. % nanocomposite. The peak values for tensile strength, impact strength, and microhardness were obtained corresponding to 1.5 wt. % clay

nanocomposite as compared to neat epoxy, followed by a decreasing trend. The tensile modulus increased till 3 wt. % clay loading, followed by a decreasing trend whereas the tensile strain at break showed a continuous decreasing trend with increasing clay content. SEM fractography of tensile fractured surfaces showed that neat epoxy exhibited smooth fracture surface, indicating brittle failure whereas that of 1.5 wt. % clay nanocomposite was rough and marked by short cracks, indicating presence of crack deflection, crack pinning, and crack arresting energy absorption mechanisms, leading to maximum enhancement of tensile strength. SEM image of 4 wt. % clay nanocomposite showed large distinct agglomerates, which acted as point of stress concentrations and decreased the tensile strength of nanocomposites. The impact fractured surface of neat epoxy was quite smooth and flat except for some river like markings, indicating brittle fracture behaviour. Fractured surface of 1.5 wt. % clay nanocomposite was rough, indicating the presence of crack deflection, crack pinning, and crack arresting mechanisms, responsible for maximum enhancement in impact strength. Moreover some of the applied energy was dissipated in plastic deformation of microvoids (generated due to debonding at clay-matrix interface) and microcracks alongwith the splitting of clay tactoids.

Chapter 5
Conclusions and Scope of Future Work

5.1 General

This chapter brings forward the conclusions from the studies regarding mechanical properties (tensile, impact and microhardness properties) of the Cloisite® 93A nanoclay-epoxy composites. The chapter also discusses the conclusions drawn with regard to the clay morphology and fractographic analysis of the composite systems. Finally, the recommendations and research areas that can be explored for future studies have been listed.

5.2 Conclusions

5.2.1 Fabrication of Epoxy-Clay Nanocomposites

- The most important parameter for obtaining improved mechanical properties in epoxy-clay nanocomposites is the diffusion of epoxy monomers into the clay galleries, leading to enhanced interfacial interactions between clay and matrix and generation of intercalated and/or exfoliated morphologies.
- Definite sequences of crucial processing steps were performed in order to obtain the desired morphology. The epoxy-clay mixture was firstly homogenized (using homogenizer at 20000 rpm), followed by ultrasonication (using probe sonicator) at 80 % amplitude control for 15 min (pulse on time = 30 s, pulse off time = 10 s). Finally, hardener was added during continuous mechanical stirring and the resulting clay-epoxy resin mixture was allowed to cure in aluminium moulds for 24 h at room temperature.

5.2.2 X-Ray Diffraction (XRD) Analysis

- The d-spacing for pristine MMT (Cloisite® 93A) was obtained 25.07 Å, which increased to 34.02 Å for 1.5 wt. % clay nanocomposite. However, at higher clay loadings (> 1.5 wt. %), the basal spacing obtained was about 32 Å (d-spacing ~ 32 Å).
- Nanocomposite containing 0.5 wt. % clay showed complete exfoliation/disordered intercalation, characterized by absence of peak in XRD diffractogram whereas, remaining

nanocomposite formulations showed only an intercalated morphology, characterized by presence of peak at a 2θ angle less than that for the pristine nanoclay.

- Cloisite® 93A is a natural montmorillonite containing no organic modifiers. Still, in the present work, intercalated and exfoliated clay morphologies were obtained in different nanocomposite formulations. Thus, the processing parameters used for homogenization and ultrasonication (rpm, time, amplitude etc.) in the experimental work were satisfactory.
- The main reasons for obtaining intercalated morphology (at clay loadings $>$ 0.5 wt. %) were attributed to the increase in viscosity of resin due to increased amount of nanoclay content in it and the strong tendency of nanoclay particles to agglomerate. It was also inferred that the elastic forces acting between the clay galleries (responsible for clay exfoliation) were not able to overcome the extra-gallery viscous forces and van der Waal attractive forces, leading to the generation of intercalated morphology rather than exfoliated morphology.

5.2.3 Tensile Properties Analysis

A) Tensile Modulus

- Tensile modulus of the pure polymer was 2576 MPa which got increased to 4200 MPa for 3 wt. % clay nanocomposite (signifying an enhancement of about 63 %) and was then followed by a decreasing trend.
- Improvement in tensile modulus was attributed to the good dispersion of nanoparticles in the epoxy matrix, which restricted the mobility of polymer chains under loading due to the good interfacial adhesion between the nanoclay and epoxy matrix. Further, the modulus of a composite depends upon the ratio of filler modulus to matrix material modulus. Since montmorillonite has a higher modulus, hence the modulus of nanocomposite system increased upto 3% loading. Beyond this clay loading, the decrease in tensile modulus was attributed to clay agglomerations, leading to decrease in polymer-clay surface interactions.

B) Tensile Strength

- Tensile strength of the neat epoxy was 36.30 MPa which increased to 53.72 MPa for 1.5 wt. % clay nanocomposite (signifying an improvement of about 48 %) and was then followed by a decreasing trend.
- Improvement in tensile strength was observed because of the high aspect ratio of nanoclay, which increased the nanofiller contact surface area on the polymer matrix. Also, the large number of reinforcing nanoclay platelets present in the polymer matrix acted as efficient stress transfer agents in the nanocomposites, inducing plastic deformation into the base polymer. Decrease in strength after 1.5 wt. % clay loading was attributed to factors viz. weak boundaries between nanoclay particles and microsized air bubbles entrapped during the sample preparation; inhomogeneous network density of samples due to increased mixture viscosity at higher clay loadings leading to heterogeneity in the resultant samples; small degassing periods due to less gel time, thus hindering the complete removal of air bubbles from nanocomposite formulations leading to generation of material defects (voids, holes etc., probably left by a gas bubble).

C) Strain at break

- The maximum value observed for strain at break was 1.7 % for the pure epoxy sample, which reduced to 1.1 % at 4 wt. % clay loading which signified about 54 % reduction in strain at break.
- This decrement in strain at break could be attributed to the fact that clay particles are rigid fillers, which make the nanocomposite more brittle at high clay contents, reducing the matrix deformation considerably.

D) SEM Analysis of Tensile Specimens

- SEM image of fractured surface of neat epoxy resin exhibited a relatively smooth surface with occasional river patterns, representing brittle fracture behaviour. Two distinct regions (Region A and Region B) were identified and it was observed that the cracks first initiated in Region A, leaving smooth appearance due to slow advance rate. However, upon reaching critical crack size, they propagated at a high rate and resulted in a coarse surface of Region B.
- The fractured surface of 1.5 wt. % clay nanocomposite was rough displaying a marked departure from the smoother brittle cleavage type fracture for neat epoxy. The cracks

were fine, close, short, twisting, varying in shape, and scattered in various directions. Moreover, energy absorption mechanisms like crack deflection, crack pinning, and crack arresting played a major role in enhancing the tensile strength of 1.5 wt. % clay nanocomposite.

- The fractured surface of 4 wt. % clay nanocomposite showed large clay agglomerates leading to low polymer-clay surface interactions and stress concentration effects, explaining the reason for obtaining lowest values of tensile properties (tensile strength, modulus and strain at break) at this particular composition.

5.2.4 Impact Strength Analysis

- Impact strength of the neat epoxy was 1.32 kJ/m^2, which got increased to 1.61 kJ/m^2 for 1.5 wt. % nanocomposite, signifying an improvement of about 22 %.
- The intercalated nanoclay particles seem to act as crack stoppers and form torturous crack propagation path, resulting in higher impact energy.

A) SEM Analysis of Impact Specimens

- Fractured surface of neat epoxy was observed to be quite smooth, indicating brittle fracture behaviour corresponding to poor impact strength.
- In 1.5 wt. % clay nanocomposite, energy absorption mechanisms like crack deflection, crack pinning and crack arresting led to torturous path followed by crack before failure, responsible for high impact strength. Also a few clay aggregates were observed, which readily interacted with the growing crack front, causing perturbations along the crack front.
- Some of the applied energy was dissipated by the deformation of microvoids (generated due to debonding of the clay-matrix interfacial region), microcracks and splitting of clay tactoids, contributing to an increase in impact resistance.

5.2.5 Microhardness Analysis

- Microhardness value for neat epoxy was observed to be 31.7 Hv, which increased to 45.8 Hv, representing an improvement of about 44.5 %.
- Intrinsic good hardness of MMT and good interfacial adhesion between nanoclay and epoxy led to better resistance against epoxy segment motion upon application of load, leading to maximum enhancement of microhardness at 1.5 wt. % nanoclay loading.

- Higher clay loadings (> 1.5 wt. % clay) retarded the chemical reaction thus, leading to incomplete curing and softening of the matrix, which could be held responsible for decreased microhardness values.

5.3 Major Conclusions and Scope of Future Work

- The present work focused upon the synthesis, characterization and study of mechanical behaviour of epoxy-clay nanocomposites. It was observed that the maximum enhancement of tensile strength, impact strength, and microhardness was obtained corresponding to 1.5 wt. % nanoclay loading as compared to neat epoxy, followed by a decreasing trend. Tensile modulus increased till 3 wt. % nanoclay loading, followed by a decreasing trend whereas tensile strain at break showed a continuous decreasing trend with increasing clay content.
- The current study can further be expanded to the areas of thermal property analysis like thermogravimetric analysis (TGA, used to quantify thermal stability and weight loss characteristics of different epoxy-clay formulations) and differential scanning calorimetry (DSC, for obtaining glass transition temperature as well as to determine the extent of curing in different epoxy-clay formulations).
- Tribology is a science that deals with design, friction, wear and lubricating surfaces in relative motion. Since the predominant feature of nanoparticles lies in their ultra-fine dimension, filler atoms can reside at the interface and lead to a strong interfacial interaction of the nanofillers, it they are well dispersed. As a result, the nanocomposites coupled with a great number of interfaces could be expected to provide exceptional tribological performance. Hence, tribological analysis could be performed by studying the dry sliding wear behaviour of MMT filled nanocomposites.
- Presence of layered silicates hinders the diffusion of solvent molecules and increases the tortuosity path, making the diffusion of solvent molecules a time consuming process thereby improving the barrier properties. Hence, barrier properties of different epoxy-clay formulations could be analyzed in terms of water, acetone, acid, base or crude oil uptake.
- Moreover, the incorporation of a tertiary filler, in the form of thermoplastic modifiers like high-impact polystyrene (HIPS) and poly(methyl methacrylate) (PMMA); impact modifiers like polyether polyol; and liquid rubber like poly(butadiene-co-acrylonitrile) (CTBN) may give more enhanced properties as compared to binary nanocomposite systems.

- Other than impact strength, fracture toughness test (using ASTM D5045–99, which is a standard test method for plain-strain fracture toughness and strain energy release rate of plastic materials) can be performed in order to study the toughening effect of nanoclay particles in epoxy matrix.
- Variables such as speed of homogenizer, amplitude of ultrasonication etc. could also be varied in order to study their effect on the properties of epoxy-clay nanocomposite formulations.

References

- Abacha N, Kubouchi M, Tsuda K, Sakai T. Performance of epoxy-nanocomposite under corrosive environment. eXPRESS Polymer Letters 2007; 1(6): 364–369.
- Abot JL, Yasmin A, Daniel IM. Mechanical and thermoviscoelastic behaviour of clay/epoxy nanocomposites. MRS Online Proceedings Library. Materials Research Society Symposium Proceedings 740; 2002 Dec 2–6; Boston (Massachusetts). Warrendale: Pennsylvania; 2003. p 75–80.
- Alexandre M, Dubois P. Polymer-layered silicate nanocomposites: preparation, properties and uses of a new class of materials. Materials Science and Engineering 2000; 28: 1–63.
- Al-Qadhi M, Merah N, Gasem ZM, Abu-Dheir N, Aleem BJA. Effect of water and crude oil on mechanical and thermal properties of epoxy-clay nanocomposites. Polymer Composites 2014; 35: 318–326.
- Al-Qadhi M, Merah N, Gasem ZM. Mechanical properties and water uptake of epoxy-clay nanocomposites containing different clay loadings. Journal of Materials Science 2013; 48: 3798–3804.
- Akbari B, Bagheri R. Deformation mechanism of epoxy/clay nanocomposite. European Polymer Journal 2007; 43: 782–788.
- Auad ML, Nutt SR, Pettarin V, Frontini PM. Synthesis and properties of epoxy-phenolic clay nanocomposites. eXPRESS Polymer Letters 2007; 1: 629–639.
- Azeez AA, Rhee KY, Park SJ, Hui D. Epoxy clay nanocomposites-processing, properties and applications: A review. Composites 2013; 45: 308–320.
- Babayan EP, Nyugen XH, inventors; Fiberite Inc., assignee. Epoxy Matrix Toughened with Polyimide Thermoplastic Resin. European Patent 0 455 755 B1. 1997 April 2.
- Bakar M, Białkowska A, Molenda J, Piasek J. Preparation and properties evaluation of thermoplastic modified epoxy nanocomposites. Journal of Macromolecular Science, Part B: Physics 2012; 51: 1159–1171.
- Basara C, Yilmazer U, Bayram G. Synthesis and characterization of epoxy based nanocomposites. Journal of Applied Polymer Science 2005; 98: 1081–1086.

- Bashar M, Mertiny P, Sundararaj U. Effect of nanocomposite structures on fracture behaviour of epoxy-clay nanocomposites prepared by different dispersion methods. Journal of Nanomaterials 2014; 2014: 1–12. (http://dx.doi.org/10.1155/2014/312813)
- Callister W. Material science and engineering an introduction. 7th ed. USA: John Wiley & Sons; 2007.
- Camargo P, Satyanarayana K, Wypych F. Nanocomposites: synthesis, structure, properties and new application opportunities. Materials Research 2009, 12: 1–39.
- Chozan CK, Rajasekaran R, Alagar M, Gnanasundaram P. Thermomechanical behaviour of vinyl ester oligomer-toughened epoxy-clay hybrid nanocomposites. International Journal of Polymeric Materials and Polymeric Biomaterials 2008; 57: 319–337.
- Dasari A, Yu ZZ, Mai YW, Hu GH, Varlet J. Clay exfoliation and organic modification on wear of nylon 6 nanocomposites processed by different routes. Composites Science and Technology 2005; 65: 2314–2328.
- Giannis S, Adams RD, Clark LJ, Taylor MA. The use of a modified peel specimen to access the peel resistance of aircraft fuel tank sealants. International Journal of Adhesion and Adhesives 2008; 28: 158–175.
- Gupta N, Lin TC, Shapiro M. Clay/epoxy nanocomposites: processing and mechanical properties. The Journal of the Minerals, Metals & Material Society 2007; 59: 61–65.
- Harris B. Engineering composite materials. 2nd ed. Institute of Materials; 1999.
- Hule RA, Pochan DJ. Polymer nanocomposites for biomedical applications. MRS BULLETIN 2007; 32: 354–358.
- Hwang SY, Lee WD, Lim JS, Park KH, IM SS. Dispersibility of clay and crystallization kinetics for *in situ* polymerized PET/ pristine and modified montmorillonite Nanocomposites. Journal of Polymer Science; 46: 1022–1035.
- Isik I, Yilmazer U, Bayram G. Impact modified epoxy/montmorillonite nanocomposites: synthesis and characterization. Polymer 2003; 44: 6371–6377.
- Khanbabaei G, Aalaie J, Rahmatpour A, Khoshniyat A, Gharabadian MA. Preparation and properties of epoxy-clay nanocomposites. Journal of Macromolecular Science, Part B: Physics 2007; 46: 975–986.

- Kim JK, Mai YW. Engineered interfaces in fiber reinforced composites. 1st ed: Elsevier; 1998.
- Kotsilkova R, editor. Thermoset nanocomposites for engineering applications. United Kingdom: Smithers Rapra Technology Limited; 2007.
- Kumar MSS, Raju NMS, Sampath PS, Vivek U. Tribological analysis of nano clay/ epoxy/ glass fiber by using Taguchi's technique. Materials and Design 2015; 70: 1–9.
- Kurahatti RV, Surendranathan AO, Kori SA, Singh N, Kumar AVR, Srivastava S. Defence applications of polymer nanocomposites. Defence Science Journal 2010; 60: 551–563.
- Kusmono, Wildan MW, Ishak ZAM. Preparation and properties of clay-reinforced Epoxy nanocomposites. International Journal of Polymer Science 2013; 2013: 1–7. (http://dx.doi.org/10.1155/2013/690675)
- Lam CK, Cheung H, Lau K, Zhou L, Ho M, Hui D. Cluster size effect in hardness of nanoclay/epoxy composites. Composites: Part B 2005; 36: 263–269.
- Li X, Zhan Z, Peng G, Wang W. A new method for preparing completely exfoliated epoxy/clay nanocomposites: nano-disassembling method. Polymer Bulletin 2011; 67: 719–727.
- Lim SR, Chow WS. Fracture toughness enhancement of epoxy by organo-montmorillonite. Polymer-Plastics Technology and Engineering 2011; 50: 182–189.
- Lingaraju D, Ramji K, Devi MP, Lakshmi UR. Mechanical and tribological studies of polymer hybrid nanocomposites with nano reinforcements. Bulletin of Materials Science 2011; 34: 705–712.
- Liu T, Tjiu WC, Tong Y, Chaobin H, Goh SS, Chung TS. Morphology and fracture behaviour of intercalated epoxy/clay nanocomposites. Journal of Applied Polymer Science 2004; 94: 1236–1244.
- Mallick PK. Fiber reinforced composites materials, Manufacturing and Design. 3rd ed. CRC Press; 2007.
- Mohan TP, Kumar MR, Velmurugan R. Mechanical and barrier properties of epoxy polymer filled with nanolayered silicate clay particles. Journal of Materials Science 2006; 41: 2929–2937.

- Morgan AB. Additives, Nanocomposites and Barrier Coatings. In: Pochiraju, Kishore V, Tandon, Gyaneshwar, Schoeppner, Gregory A, editors. Long-term durability of polymeric matrix composites. 1st ed. United States: Springer; 2012. p 39–75.
- Mouloud A, Cherif R, Fellahi S, Grohens Y, Pillin I. Study of morphological and mechanical performance of amine-cured glassy epoxy-clay nanocomposites. Journal of Applied Polymer Science 2012; 124: 4729–4739.
- Ngo TD, That MTT, Hoa SV, Cole KC. Preparation and properties of epoxy nanocomposites. part 2: the effect of dispersion and intercalation/exfoliation of organoclay on mechanical properties. Polymer Engineering and Science 2012; 52: 607–614.
- Nikje MMA, Khanmohammad M, Garmarudi AB, Ghasemi K. Analysis of variance (ANOVA) for optimizing the nano-SiO_2 content of high performance epoxy nanocomposites. Journal of Macromolecular Science, Part-A: Pure and Applied Chemistry 2009; 46: 116–120.
- Olad A, Azar RH, Babaluo AA. Investigation on the mechanical and thermal properties of intercalated epoxy/layered silicate nanocomposites. International Journal of Polymeric Materials 2012; 61: 1035–1049.
- Park JH, Jana SC. Mechanism of exfoliation of nanoclay particles in epoxy-clay nanocomposites. Macromolecules 2003; 36: 2758–2768.
- Rashmi, Renukappa NM, Suresha B, Devarajaiah RM, Shivakumar KN. Dry sliding wear behaviour of organo-modified montmorillonite filled epoxy nanocomposites using Taguchi's techniques. Materials and Design 2011; 32: 4528–4536.
- Raturi M. Fabrication and property evaluation of a epoxy-clay-PET nanocomposite system [dissertation]. Patiala: Thapar Univ; 2014.
- Ray SS and Okamoto Masami. Polymer/layered silicate nanocomposites: a review from preparation to processing. Progress in Polymer Science 2003; 28: 1539–1641.
- Sánchez-Cabezudo M, Prolongo MG, Salom C, García del Cid MA, Masegosa RM. Ternary nanocomposites: curing, morphology, and mechanical properties of epoxy/ thermoplastic/ organoclay systems. Polymer Composites 2015; 00: 000–000. (DOI 10.1002/pc.23397)

- Sharmila TKB, Ayswarya EP, Abraham BT, Begum PMS, Thachil ET. Fabrication of partially exfoliated and disordered intercalated cloisite epoxy nanocomposites via in situ polymerization: mechanical, dynamic mechanical, thermal and barrier properties. Applied Clay Science 2014; 102: 220–230.
- Smith WF, Hashemi J. Materials science and engineering. 4th ed. New Delhi: Tata McGraw Hill Education Private Limited; 2008.
- Teh SF, Liu T, Wang L, He C. Fracture behaviour of poly(ethylene terephthalate) fiber toughened epoxy composites. Composites: Part A 2005; 36: 1167–1173.
- Toldy A, Szolnoki B, Marosi G. Flame retardancy of fiber-reinforced epoxy resin composites for aerospace applications. Polymer Degradation and Stability 2011; 96: 371–376.
- Tsai TY, Kang HC, Yin MS, Hsu KY, Jong SJ, inventors; Industrial Technology Research Institute, assignee. Modified layered clay material and epoxy/clay nanocomposite containing the same. US patent US 2003/0039835 A1. 2003 Feb 27.
- Wang K, Chen L, Wu J, Toh ML, He C, Yee AF. Epoxy nanocomposites with highly exfoliated clay: mechanical properties and fracture mechanisms. Macromolecules 2005; 38: 788–800.
- Wang K, Wang L, Wu J, Chen L, He C. Preparation of highly exfoliated epoxy/ clay nanocomposites by “slurry compounding”: process and mechanisms. Langmuir 2005; 21: 3613–3618.
- Wang Z, Gu P, Wu X, Zhang H, Zhang Z, Chiang MYM. Micro/nano-wear studies on epoxy/silica nanocomposites. Composites Science and Technology 2013; 79: 49–57.
- Yasmin A, Abot JL, Daniel IM. Processing of clay/epoxy nanocomposites with a three-roll mill machine. MRS Online Proceedings Library. Materials Research Society Symposium Proceedings 740; 2002 Dec 2–6; Boston (Massachusetts). Warrendale: Pennsylvania; 2003. p 75–80.
- Ying Z, Xianggao L, Bin C, Fei C, Jing F. Highly exfoliated epoxy/clay nanocomposites: mechanism of exfoliation and thermal/mechanical properties. Composite Structures 2015; 132: 44–49.

- Zaarei D, Sarabi AA, Sharif F, Gudarzi MM, Kassiriha SM. The impact of organoclay on the physical and mechanical properties of epoxy-clay nanocomposite coatings. Journal of Macromolecular Science, Part B: Physics 2010; 49: 960–969.
- Zunjarrao SC, Sriraman R, Singh RP. Effect of processing parameters and clay volume fraction on the mechanical properties of epoxy-clay nanocomposites. Journal of Materials Science 2006; 41: 2219–2228.

Web References

- http://nptel.ac.in/ (visited on 3rd October, 2013)
- http://www.nanoshel.com/product/cloisite-93a-montmorillonite-nano-powderspurity-99-aps/ (visited on 18th August, 2014)
- http://www.jeol.com (visited on 15th October, 2014)
- http://www.ika.com/Dispersing_appl-5.html (visited on 2nd November, 2014)
- http://www.macroscientificworks.com/ovens-incubators8.html#ove8 (visited on 7th November, 2014)
- http://www.panalytical.com/XPert3-Powder/Specifications.htm (visited on 19th January, 2015)
- http://www.sonicator.com/literature/how-it-works.shtml (visited on 13th March, 2015)
- http://senselektro.hu/wp-content/uploads/zwick/ProLine.pdf (downloaded on 30th April, 2015)
- http://www.remilabworld.com/Direct_Drive_Stirrers.asp (visited on 23rd May, 2015)
- http://ipelican.com/en/131570 (visited on 11th June, 2015)
- http://www.metatechind.com/html/micro.htm (visited on 29th June, 2015)

ANNEXURE-I

Sample Code	Tensile Modulus (MPa)	Tensile Strength (MPa)	Strain at break (%)
Composition: C0 (pristine epoxy with 0 wt. % clay content)			
T1	2720	34.6	1.8
T2	2510	32.5	1.7
T3	2490	41.2	1.6
T4	2950	37.5	1.6
T5	2210	35.7	1.8
Composition: C0.5 (nanocomposite with 0.5 wt. % clay content)			
T1	4170	55.4	1.6
T2	4080	50.4	1.5
T3	3880	48.6	1.5
T4	3670	47.3	1.6
T5	3950	43.1	1.5
Composition: C1 (nanocomposite with 1 wt. % clay content)			
T1	4570	50.3	1.4
T2	3710	48.9	1.3
T3	3930	53.1	1.5
T4	4010	55.5	1.5
T5	—	—	—
Composition: C1.5 (nanocomposite with 1.5 wt. % clay content)			
T1	4630	51.1	1.4
T2	3950	55	1.3

T3	3850	54.5	1.5
T4	4160	58.3	1.3
T5	3780	49.7	1.3
Composition: C2 (nanocomposite with 2 wt. % clay content)			
T1	4260	36.2	1.2
T2	3910	34.3	1.2
T3	4380	31.5	1.0
T4	4110	37.9	1.3
T5	3880	32.1	1.0
Composition: C3 (nanocomposite with 3 wt. % clay content)			
T1	4170	30	1.0
T2	4460	35.9	1.2
T3	4480	37	1.1
T4	3800	28.3	1.1
T5	4090	27.9	1.1
Composition: C4 (nanocomposite with 4 wt. % clay content)			
T1	3470	37.6	1.2
T2	3100	33.7	1.0
T3	4250	33	1.2
T4	3970	30.8	1.0
T5	3530	23.8	1.1

‘—‘: Sample damaged during cutting

ANNEXURE-II

SAMPLE CODE	IMPACT STRENGTH (kJ/m^2)				
	I1	**I2**	**I3**	**I4**	**I5**
C0.0 (0.0 wt. % nanoclay)	1.35	1.29	1.35	—	1.31
C0.5 (0.5 wt. % nanoclay)	1.36	1.36	1.38	1.39	1.34
C1.0 (1.0 wt. % nanoclay)	1.55	1.63	1.58	1.57	1.61
C1.5 (1.5 wt. % nanoclay)	1.61	1.59	1.65	1.58	1.63
C2.0 (2.0 wt. % nanoclay)	—	1.59	1.56	1.62	1.52
C3.0 (3.0 wt. % nanoclay)	1.35	1.35	1.44	1.39	1.42
C4.0 (4.0 wt. % nanoclay)	1.36	1.29	1.31	1.26	1.44

'—': Outlier

ANNEXURE-III

Serial No.	C0.0 (Hv)	C0.5 (Hv)	C1.0 (Hv)	C1.5 (Hv)	C2.0 (Hv)	C3.0 (Hv)	C4.0 (Hv)
1	32.37909	37.08800	47.32663	54.30055	44.07154	38.34513	42.90413
2	28.72095	41.78251	48.66916	49.72463	46.12589	38.99780	34.47599
3	34.47599	35.03204	49.59617	48.78646	40.35415	38.02493	37.08800
4	38.66940	49.25219	44.40208	39.33041	44.47128	41.05901	40.35415
5	34.75235	29.35799	35.04819	45.28725	51.18348	36.18528	34.47599
6	31.40166	39.66728	41.37986	48.32729	49.72464	39.66728	33.14242
7	22.45657	38.02493	38.65603	41.41839	43.85379	40.70429	41.05901
8	30.01670	33.93307	46.46223	44.87648	37.08810	40.00850	36.18528
9	33.14242	34.75235	47.76790	41.78251	52.19199	38.99780	38.99780
10	30.01647	40.00850	35.32914	49.72464	38.99780	41.05901	32.63057
11	20.18908	38.34513	32.16700	47.42820	50.20931	41.41839	42.15144
12	32.37909	38.66940	38.65603	43.28806	41.78251	43.67717	42.52529
13	31.40166	45.20937	42.10581	37.08800	49.25220	36.18528	41.78251
14	33.93307	35.32914	45.62130	42.52529	48.32729	34.47599	35.60166
15	31.64183	44.40208	44.00652	46.55396	44.07154	43.28806	40.00850
16	30.92946	40.32565	40.32565	52.70746	40.23851	42.15144	34.75235
17	30.46784	45.62131	44.80300	45.70368	49.25220	44.47128	41.41839
18	33.14242	35.90126	44.40208	49.82362	41.09501	40.00850	40.70429
19	38.34513	42.85103	48.66916	50.96613	37.39642	42.90413	36.18528
20	37.39642	36.48739	50.06964	47.88931	47.42820	36.18528	33.14242